Accepted Manuscript

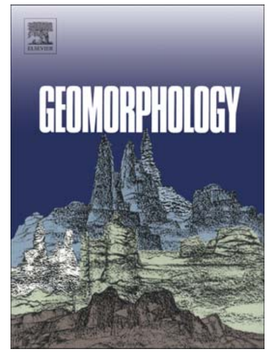

Exhumation and incision history of the Lahul Himalaya, northern India, based on (U-Th)/He thermochronometry and terrestrial cosmogenic nuclide methods

Byron Adams, Craig Dietsch, Lewis A. Owen, Marc W. Caffee, James Spotila, William C. Haneberg

PII: S0169-555X(08)00553-9
DOI: doi: 10.1016/j.geomorph.2008.12.017
Reference: GEOMOR 2843

To appear in: *Geomorphology*

Received date: 12 September 2008
Revised date: 19 December 2008
Accepted date: 22 December 2008

Please cite this article as: Adams, Byron, Dietsch, Craig, Owen, Lewis A., Caffee, Marc W., Spotila, James, Haneberg, William C., Exhumation and incision history of the Lahul Himalaya, northern India, based on (U-Th)/He thermochronometry and terrestrial cosmogenic nuclide methods, *Geomorphology* (2009), doi: 10.1016/j.geomorph.2008.12.017

Exhumation and incision history of the Lahul Himalaya, northern India, based on (U-Th)/He thermochronometry and terrestrial cosmogenic nuclide methods

Byron Adams[a], Craig Dietsch[a*], Lewis A. Owen[a], Marc W. Caffee[b], James Spotila[c], William C. Haneberg[d]

[a] *Department of Geology, University of Cincinnati, P.O. Box 0013, Cincinnati, OH 45221-0013, U.S.A.*

[b] *Dept of Physics/PRIME Laboratory, Purdue University, West Lafayette, IN 47906, USA*

[c] *Department of Geosciences, Virginia Tech, Blacksburg, VA 24061, USA*

[d] *Haneberg Geoscience, 10208 39th Avenue SW, Seattle WA 98146, USA*

Corresponding author:
Craig Dietsch
telephone 513.556.2547
FAX 513.556.6931
craig.dietsch@uc.edu

Abstract

Low-temperature apatite (U-Th)/He (AHe) thermochronology on vertical transects of leucogranite stocks and ^{10}Be terrestrial cosmogenic nuclide (TNC) surface exposure dating on strath terraces in the Lahul Himalaya provide a first approximation of long-term (10^4 - 10^6 years) exhumation rates for the High Himalayan Crystalline Sequence (HHCS) for northern India. The AHe ages show that exhumation of the HHCS in Lahul from shallow crustal levels to the surface was ~ 1-2 mm/a and occurred during the past ~ 2.5 Ma. Bedrock exhumation in Lahul fits into a regional pattern in the HHCS of low-temperature thermochronometers yielding Plio-Pleistocene ages. Surface exposure ages of strath terraces along the Chandra River range from ~ 3.5 to 0.2

ka. Two sites along the Chandra River show a correlation between TCN age and height above the river level yielding maximum incision rates of 12 and 5.5 mm/a. Comparison of our AHe and surface exposure ages from Lahul with thermochronometry data from the fastest uplifting region at the western end of the Himalaya, the Nanga Parbat syntaxis, illustrates that there are contrasting regions in the High Himalaya where longer term (10^5 – 10^7 years) erosion and exhumation of bedrock substantially differ even though Holocene rates of fluvial incision are comparable. These data imply that the orogen's indenting corners are regions where focused denudation has been stable since the mid-Pliocene. However, away from these localized areas where there is a potent coupling of tectonic and surface processes that produce rapid uplift and denudation, Plio-Pleistocene erosion and exhumation can be characterized by disequilibrium, where longer term rates are relatively slower and shorter term fluvial erosion is highly variable over time and distance. The surface exposure age data reflect differential incision along the length of the Chandra River over millennial time frames, illustrate the variances that are possible in Himalayan river incision, and highlight the complexity of Himalayan environments.

Keywords: Himalaya; strath terraces; terrestrial cosmogenic nuclides; AHe thermochronology; exhumation; fluvial incision; Lahul

1. Introduction

Processes at convergent plate boundaries that build topography are widely understood to be episodic on timescales of 10^6-10^7 years (for example, Lamb et al., 1997; Lister et al., 2001; Quarles van Ufford and Cloos, 2004). Transient landscapes, too, can persist on time scales of 10^6 years (Kirby et al., 2002; Clark et al., 2006; Riihimaki, 2007). How erosion responds to changes in uplift, whether erosion rates vary with time, and whether mountain landscapes are transient or can achieve steady-state conditions remain important questions in geomorphology. Key processes in addressing these issues are exhumation and erosion. The rates of these processes constrain the interplay and relative roles of tectonic *vs.* surficial geologic processes in mountain belts.

The Himalayan orogen is an archetype natural laboratory for the study of exhumation and erosion because it is tectonically active and characterized by extreme relief (relative relief can exceed 3000 m), large-scale mass wasting (large avalanches, debris flows, and rock falls), and glacial landforms (over steepened valleys, moraines, and glacial dam bursts). Exhumation rates of the northern Indian Himalaya have not been well defined in spite of their significance for surficial and tectonic dynamics. To further understand the timing and rates of exhumation and erosion in the Lahul region of the Greater Himalaya, we have obtained quantitative data using (U-Th)/He apatite (AHe) thermochronology and terrestrial cosmogenic nuclide (TCN) methods.

Lahul is located approximately midway between the Indo-Gangetic Plain and Tibet (Fig. 1) in the Pir Panjal and Greater Himalaya of northern India. Lahul is an impressive, rugged landscape comprising U-shaped valleys, mountain sides and peaks underlain by massively jointed faces of granite, large granite and meta-sedimentary debris deposits, and smaller fluvial and glacial landforms.

Several general aspects of the exhumation history of the Lahul Himalaya are well characterized. These are derived from studies of regional deformation and faulting (Steck et al., 1993; Vannay and Steck, 1995; Wyss and Steck, 1999), chronology of emplacement of igneous rocks and regional metamorphism (Searle and Fryer, 1986; Walker et al., 1999), and geomorphic evolution (Owen et al., 1995, 1997, 2001). Some specific aspects of erosion in Lahul have been studied, including catastrophic flooding (Coxon et al., 1996), glaciation, and paraglaciation (Owen et al., 1995). However, results from these studies are too spatially or temporally narrow to define regional exhumation or erosion rates. Moreover, longer-term exhumation and erosion rates, on timescales of 10^5-10^7 years, are lacking from Lahul. Recent thermochronologic studies elsewhere in the Himalaya have defined exhumation rates of 3-7 mm/a at time scales of 10^6 years (Harrison et al., 1997; Zeitler et al., 2001). Fission track (FT) data have revealed that significant erosion occurred in the Pakistan Karakoram during the Pliocene. Foster et al. (1994) proposed that at least 7000 m of rock were eroded during this period, yielding exhumation rates of 3-6 mm/a.

To build on these studies, we employed low-temperature AHe thermochronology on vertical transects of leucogranite stocks and ^{10}Be terrestrial cosmogenic nuclide (TCN) surface exposure dating (SED) on strath terraces exposed along the Chandra River and one of its tributaries. Our primary goals in using AHe thermochronology in Lahul were first, to determine whether long-term (10^6 years) exhumation rates could be established, and second, to gather data bearing on whether the topographic and thermal structure of Lahul have reached steady-state. Changes in erosion rate and the rate at which topography develops can significantly affect the migration and geometry of isotherms and can disturb cooling ages at the surface (Braun et al., 2006, p.105-176). TNC methods can quantify surface processes at millennial timescales back to 20-30 ka, and our goal of dating strath terraces was to determine recent river incision rates. Any spatial and temporal variation in surface exposure ages of strath terraces along the Chandra will provide a gauge of the heterogeneity of fluvial bedrock incision in this active Himalayan environment.

Our data can be used to test whether the Lahul Himalaya has undergone rapid exhumation. i.e. 3-7 mm/a, as proposed for elsewhere in the orogen and to determine whether local river incision rates are as high as other regions of the Himalaya, of the order of 1 to 20 mm/a, where more is known about uplift and erosion histories (Burbank et al., 1996). The timing of low-temperature cooling and the fluvial incision of the High Himalayan Crystalline Sequence (HHCS) in Lahul further bears on the linkage between local topography, regional rock deformation and strain partitioning, and surface erosion.

2. Background

Two main NW-SE-trending mountain ranges traverse Lahul, the Pir Panjal to the south and the Greater Himalaya to the north (Fig. 1). Both ranges include peaks exceeding 6000 m in elevation above sea level (asl; the highest peak in Lahul is Mulkila at 6520 m asl) and valley floors occur at elevations ≤ 3000 m asl.

2.1 Tectonic setting

Traversing Lahul is part of the HHCS (Vannay and Steck, 1995), the crystalline core of the orogen where mountain peaks along its entire length through the orogen are typically in excess of 6000 m asl. The HHCS in Lahul is composed of Precambrian and Paleozoic metamorphic rocks intruded by large stocks and sills of porphyritic K-feldspar granite of Cambrian-Ordovician age (Frank et al., 1973; Miller et al., 2001) and leucogranite of Miocene age (Fig. 2; Searle and Fryer, 1986; Searle, 1991; Walker et al., 1999; Webb et al., 2007). Crustal thickening in Lahul has been viewed as occurring during emplacement of southwest-verging nappes during the late Eocene to early Oligocene, and again during the late Oligocene and early Miocene coincident with movement along the northwest-dipping Main Central thrust

(MCT; Vannay and Steck, 1995). Nappe emplacement produced regional Barrovian metamorphism, dated in northwest Lahul by U-Pb ages of monazite at 29-31 Ma (Walker et al., 1999). Partial melting of metasediments during upper amphibolite facies metamorphism produced stocks and plugs, and lit-par-lit intrusion of leucogranite, resulting in widespread stromatic migmatitic layering within the metasedimentary bedrock of Lahul (Searle and Fryer, 1986). From leucogranites in Lahul, Walker et al. (1999) reported U-Pb ages of monazite, xenotime, and uraninite which together gave an age of 21 Ma; Searle and Fryer (1986) reported a muscovite Rb-Sr age of 17.6 Ma; and Vannay and Steck (1995) reported an $^{40}Ar/^{39}Ar$ age of biotite of 16 Ma, all of which record Miocene crystallization and cooling. Along-strike east of Lahul, U-Pb zircon ages of leucogranite that intrudes the HHCS are early Miocene (22-23 Ma) and middle Miocene (12-13 Ma; summarized by Hodges, 2000).

Webb et al. (2007) recently mapped the bedrock within Lahul, including our study area showing that rocks of the HHCS are in contact with the Tethyan Himalayan Sequence along the South Tibetan Detachment (STD; Fig. 2), and proposed that movement along the STD was south- and north-verging. Hodges (2006) placed the structural evolution of the HHCS in the context of the hypothesis of channel flow.

2.2 Fluvial landscape setting

Lahul lies in the transition zone between the lush monsoonal climate on the southern flanks of the Pir Panjal and the semi-arid Zanskar and Ladakh ranges of the Trans-Himalaya to the north (Fig. 3). Lahul presently receives some precipitation during the South Asian Monsoon (SAM; Benn and Owen, 1998), although this amount has not been quantified since spatial coverage of meteorological data collection stations is lacking. The annual precipitation in the semi-arid environment of Lahul is considerably less than that in the Lesser Himalaya due to orographic effects.

The Chandra and Bhaga Rivers are the principal drainages of this region and they have many smaller tributary streams originating from the surrounding steep mountainsides (Fig. 1). Within the study region, the Chandra River's stream order is a 3 on the Strahler scale as derived from a 1:250,000 scale map. The Chandra River flows down large and wide glaciated valleys that change direction nearly 180° from a SSE flow at the headwaters near Baralacha La to a range-parallel NW flow near Koksar, suggesting that the northern reaches of the Chandra Valley is antecedent while the southern portion follows topography or geologic strike. The majority of the valleys in Lahul are glaciated and U-shaped with broad floors, steep sides, and propagating debris fans. The combination of these glaciated valleys produces dramatic horns and arêtes throughout the region.

Owen et al. (1995) described the drainage system of Lahul, showing that the Lahul fluvial regime is dominated by glacial meltwater dynamics, producing large diurnal and seasonal fluctuations in discharge. Superimposed on this varying flow regime are the effects of low-frequency, high-magnitude storm flows created by occasional penetration of monsoonal airflows. The distinct daily discharges reflect diurnal temperature cycles, lagging by 3 to 5 hours. A gauging station was active during September 1993 measuring the discharge of the Chandra River at Batal. Measured discharge and stream power were 12.8 m^3/s and 3287 W/m, respectively. Stream power per unit width was 142.9 W/m^2, indicating a high bedload capacity even at low flow, non-monsoon conditions. A gauging station was also set up in a smaller tributary directly to the east of Batal, the Kharcha Valley, during September 1993. Data collected in the Kharcha

Valley show insignificant bedload transport between high magnitude monsoon storm events and the beds are clearly armored during this time. However, the data gathered at these stations are limited, as only one month was recorded.

Lahul is similar to other regions of the Himalaya in that its river systems yield very high sediment loads (Owen et al., 1995). Sediment transfer is episodic and dictated by seasonal cycles, the magnitude of monsoon storm events, and the dynamics of highly active slope processes (Owen et al., 1995). The Chandra oscillates from low width, single channel conditions to wide, multi-channel braided sandur (glacial outwash plain) reaches along its length. Large sandurs occur in valley reaches of low gradient (2-15°). There are sandurs found in the upper Chandra Valley upstream from Batal and in the upper Kulti Valley. Large alluvial fans are present in Lahul with gradients of 2-10° reflecting high rates of deposition from glaciofluvial rivers. There are also fans dominated by debris flows. Exposed sections of fans exhibit interbedded sands, gravels, diamictons, and boulder layers. The presence of fan terraces implies distinct episodes of aggradation and incision (Owen et al., 1995).

2.3 Glacial landscape setting

Abundant glacial landforms show that Lahul has been extensively glaciated. Owen et al. (2001) recognized five late Quaternary glacial stages in Lahul: the Chandra and Batal glacial stages characterized by major valley glaciations, when glaciers occupied the main Chandra trunk valley; the Kulti glacial stage where glaciers occupied tributary valleys and in some cases, may have extended partially into the larger trunk valley; and the Sonapani I and II glacial stages represented by limited glacier advances with glaciers restricted to tributary valleys. The Batal and Kulti glacial stages have been dated by TCN surface exposure dating methods to 12-15.5 ka and 10–11.4 ka, respectively. The oldest and largest of the inferred glacial events, the Chandra glacial stage, produced bedrock benches and eroded drumlins at elevations > 4300 m asl (~ 1200 m above the present valley floor). Owen et al. (2001) suggest that all the Lahul glacial advances were strongly influenced by increased precipitation, as snow, during insolation maxima that enhanced monsoon activity in the region.

The recorded glacial events and subsequent fluvial drainage have removed large amounts of host meta-sedimentary rock and leucogranite from Lahul. It is possible that there were much older and more extensive periods of glaciation in this region prior to the Late Quaternary as Northern Hemisphere glaciation intensified at approximately 2.7 Ma (Clemens and Tiedemann, 1997). There is also evidence of glaciation older than 430 ka in the Ladakh Himalaya (~ 250 km north of Lahul; Owen et al., 2006) and glaciers were probably present in the Karakoram of Northern Pakistan since 720 ka (Cronin and Johnson, 1988). In Lahul, however, it is unlikely that evidence for these older glaciations is preserved in this very geomorphically dynamic landscape.

3. Methods

3.1 Field mapping

We use the mapping of Searle and Fryer (1986), Vannay and Steck (1995), Owen et al. (1995, 1997, 2001) and Webb et al. (2007) as a basis for our sample collection. The mapping was supplemented by detailed geomorphic, petrological and structural descriptions at study sites throughout our research area. Surveys of strath terraces were undertaken using a hand-held laser distance finder, an inclinometer, and a 30 m measuring tape.

3.2 DEM analysis

The best publicly available topographic data for the region consist of on-demand ASTER (Advanced Spaceborne Thermal Emission and Reflectance) satellite digital elevation models (DEMs) with 30 m cell size. Experience shows that the smallest landforms that can be identified and mapped on a DEM have characteristic lengths approximately an order of magnitude larger than the DEM cell size. Thus, a 30 m ASTER DEM is sufficient to identify landforms with lengths on the order of 300 m or more. This is too coarse for geomorphic mapping of all but very large landforms, but does provide a useful topographic framework for our work.

We obtained an ASTER DEM tile covering most of the project area and used it to extract topographic profiles at approximately equal intervals and nearly perpendicular to the Chandra River valley. Each profile was about 10 km long. Both the DEM (shown as a shaded relief image) and the profiles are shown in Fig. 4. We also created a series of standard topographic derivative maps including, for example, slope angle, aspect, roughness, curvature, but we did not find them useful for geomorphic interpretation at a scale commensurate with our study.

3.3. Sampling for AHe thermochronology

Ten samples were collected for AHe thermochronology from pl+qtz+kfs+ms±bt±tur±grt leucogranite in two tributary valleys of the Chandra River valley (the Hamptah and Chattru valleys) and from the Rohtang Pass that leads over the Pir Panjal northwards into the Chandra Valley. Sample locations and detailed descriptions of the rocks we collected are listed in Table 1 and shown in Fig. 5. The samples span elevations between about 3100 and 4000 m asl and cover two vertical transects; Fig. 6 illustrates the landscape from which we collected our AHe samples.

In the Hamptah Valley (on the south side of the Chandra valley; Fig. 6D), and the Chattru Valley (north side of the Chandra; Fig. 6B) we sampled a stock of tourmaline- and garnet-bearing leucogranite. Bedrock in the Hamptah and Chattru valleys is dominated by deformed greenschist facies meta-siltstone intruded by sills, dikes, and the stock of leucogranite; some dikes are pegmatitic and some aplitic.

On the Rohtang Pass (Fig. 6A), a major drainage divide with the Chandra River to the north and the Beas River to the south, we sampled leucogranite from road cut exposures that extend from just north of the pass to Koksar along the Chandra River. Exposed bedrock on the pass is characterized by upper greenschist and lower amphibolite facies metasediments intruded by leucogranite sills.

3.4. Sampling for 10Be TCN SED

Fifteen samples for ^{10}Be TCN surface exposure dating were collected from four strath terraces along the Chandra River between Chattru and Koksar to define downstream variations in incision, and one strath terrace along a tributary stream near its intersection with the Chandra (Figs. 5, 7). At each strath terrace site, two to four quartz-rich samples (leucogranite, meta-siltstone, or vein quartz) were collected from the different horizontal strath terrace surfaces (one per level). Details of the TCN samples we collected are given in Table 2.

The Chandra River has diurnal, seasonal and yearly fluctuations. At any given time, the “current river level” is highly dependent on the amount of glacier/snow melt, south Asian monsoon intensity, and drainage system lag time. During the summer when our samples were collected, the Chandra fluctuated by ~1 m, related to precipitation and time of day. The lowest and most constant flow conditions mostly likely occur in the winter months when there is less snow and glacial melt water. Our samples were collected at an elevated river stage. The ~1 m variation in river height contributes between about 5–10% error in the height measurement.

Sampling sites were chosen based on terrace surface morphology and characteristics. Specific locations to collect samples were selected on nearly horizontal surfaces of larger treads and terraces exhibiting polish, potholes, and small sinuous channels were preferentially sampled (Figs. 7C, 7E), as these treads have experienced less subsequent erosion since abandonment than flat, featureless treads. Terraces that showed weathering features, including rough surfaces, deep weathering pitting and exfoliation, were not sampled, nor were strath terraces that had any sediment cover.

The Chandra River has low-width single channel reaches where strath terraces are present (Fig. 7B). All sampled terraces are unpaired and were debris-free. Samples collected on both the north and south sides of the river. Across from the sampled strath terraces, the banks of the Chandra are debris-covered slopes. It is possible that all of these terraces were formed in paired successions, and since abandonment, one side of the valley has experienced mass wasting events that have obscured the adjacent set of terraces. Though these debris covers have not been dated, their presence indicates that they are long-lived relative to the geomorphic timescale (10^2 – 10^6 years) and not easily cleared, and implies that there should be evidence of debris cover on strath terrace surfaces if they were once covered. An effective mechanism to clear a bedrock terrace surface perched 10 m or higher above river level would be a catastrophic flooding event. Flood deposits along the Chandra (Coxon et al., 1996) are overlain by contemporary fan deposits.

3.5. AHe thermochronology

The low-temperature AHe thermochronometer allows recent exhumation of rocks to be quantified in terms of cooling histories, typically on million-year timescales. (U-Th)/He dating is based on the radiogenic production and thermally-controlled diffusion of ^4He within host minerals. Studies of ^4He diffusion in apatite show that helium begins to be quantitatively retained at ~ 80°C (Zeitler et al., 1987; Wolf et al., 1996; Farley, 2000). Apparent AHe cooling ages commonly correspond to effective closure temperatures of ~ 70°C, but may range from 80 to 40°C depending principally on grain size and cooling rate (Dodson, 1973; Farley, 2000; Ehlers and Farley, 2003; Reiners and Brandon, 2006).

Apatite grains were separated and loaded into platinum tubes by standard mineral separation techniques in the University of Cincinnati Heavy Mineral Laboratory. Apatite grains ≥70 μm in diameter and were screened for micro-inclusions and other crystal defects at 100x magnification. Multigrain AHe ages were measured at Virginia Tech on ~0.01-0.17 mg aliquots (Table 1). To counter the potential effect of U- and Th-bearing micro-inclusions (i.e. zircon and monazite (House et al., 1997)), fluid inclusions, or parent nuclide zonation on measured ages (Fitzgerald et al., 2006), we analyzed multiple (~ 4) replicates per sample (a total of 38 analyses for 10 samples). This enabled evaluation of sample reproducibility and identification of anomalously old outliers that probably have ^{4}He contamination. Samples were outgassed in a resistance furnace at 940˚C for 20 minutes (followed by a 20-minute re-extraction test) and analyzed for ^{4}He by isotope dilution utilizing a ^{3}He spike and quadrupole mass spectrometry. Blank level for ^{4}He detection was ~ 0.2 femtomoles. Radiogenic parent isotopes (^{238}U, ^{235}U, and ^{232}Th) were measured at Caltech using isotope dilution (^{235}U and ^{230}Th spike) and ICP mass spectrometry. Although ^{4}He is also produced by ^{147}Sm decay, it is not routinely measured because it should produce < 1% of radiogenic ^{4}He in typical apatite and should only be a factor in AHe ages when U concentrations are low (Farley and Stockli, 2002; Reiners and Nicolescu, in press).

Routine 1σ uncertainties due to instrument precision are +1-2% for U and Th content, +2-3% for He content, and +4-5% for alpha ejection correction factor based on grain dimension and shape. Cumulative analytical uncertainty is thus approximately ±10% (2σ). Age accuracy was cross-checked by measurements of known standards, principally Durango fluorapatite (30.9±1.53 Ma (1σ; n=40)), with a known age of 31.4 Ma (McDowell et al., 2005). These measurements on Durango show that reproducibility on some natural samples is comparable to that expected from analytical errors. Uncertainties for samples are reported as the observed standard deviation from the mean of individual age determinations (Table 1). Average AHe reproducibility on average ages in this study is ~ 14% (1σ), which is somewhat worse than that obtained from Durango apatite and indicative of poor apatite quality.

3.6. Surface exposure dating

The strath terrace samples were prepared in the University of Cincinnati Terrestrial Cosmogenic Nuclide Laboratory following precisely the same procedures presented in detail by Dortch et al. (2008). Measurement of $^{10}Be/^{9}Be$ ratios by accelerator mass spectrometry was undertaken at the PRIME Laboratory at Purdue University.

All ^{10}Be ages for rock samples were calculated using the CRONUS calculator (http://hess.ess.washington.edu/math/; Balco et al., 2008; Table 2). This uses the scaling factors of Stone (2000) and a sea-level low-latitude production rate of 4.98 ^{10}Be atoms/gram of quartz/year. Uncertainty associated with the different scaling models used to calculate the TCN ages for this region may result in ages of up to 20% older than ages calculated using the Lal (1991)/Stone (2002) time-independent modeling scheme (for more discussion see Owen et al., 2008). Accordingly, our ages can be considered as minimum values and our incision rates as maximum values. In addition, no correction was made for geomagnetic field variations due to the ongoing debate regarding which correction factors are most appropriate. Geomagnetic corrections on our ^{10}Be ages can change the age by up to 16%, but most ages change by $< 10\%$. Furthermore, we have not made any corrections for erosion. However, assuming that all the strath terrace surfaces that were sampled weather at a moderate rate of 5 m/Ma, a calculated age of 10 ka assuming zero terrace erosion would underestimate the true age by a maximum of 4%; an age of 20 ka by 9%; an age of 40 ka by 20% (Owen et al., 2002).

4. Results

4.1 Digital Terrain Modeling

Although we did not find the DEM or derivative products (e.g., slope angle, aspect, roughness, or curvature maps) useful for detailed geomorphic mapping in the project area, it did yield topographic profiles showing four terrace levels that can be correlated from profile to profile (Fig. 4). These terraces lie at elevations of approximately 4800 m, 4425 m, 3650 m, and 3450 m asl. The four terrace levels were identified on the westernmost profile (A-A'), where the river is most deeply incised, and then drawn across the upstream profiles for comparison. Profiles D-D', E-E', and F-F' contain several distinct terraces that are close, but distinctly different than, the elevations projected from profile A-A'. They are shown with a query in Fig. 4.

Because most of the queried terraces are slightly below the terrace elevations projected from profile A-A', it is unlikely that they reflect upstream elevation increases along the stream gradient. They may, however, indicate tectonic activity such as greater uplift or warping along more deeply incised portions of the valley, or terrace levels not apparent in the other profiles. At present, we are unable to distinguish between those two possibilities. Topographic anomalies along the north side of the Chandra valley in the vicinity of profiles C-C', D-D', and F-F', which are visible on both the shaded relief image and the profiles, appear to represent a complex of large scale landslides and alluvial fans.

4.2 AHe data

AHe ages from five leucogranite samples in the Hamptah Valley are Plio-Pleistocene (Fig. 8): 1.39±0.04 to 2.51±0.29 Ma. Replicate analyses from these samples reproduced fairly well, although each sample yielded one outlier that was significantly different from the mean (Table 1). The outliers for samples HA1, HA2, HA4, and HA5b are anomalously older than average AHe age and are probably due to the presence of undetected U- and/or Th-bearing micro-inclusions, as has been observed elsewhere (e.g. House et al., 1997). In these samples, the outliers were culled prior to the calculation of mean age. The outlier for sample HA4b was culled from the data on the basis of low U content and low He yield, similar to several samples from Rohtang Pass (see below). Curiously, average AHe ages from the Hamptah Valley (Fig. 8) do not show a positive correlation between age and elevation.

AHe ages from Rohtang Pass and Chattru Valley reproduced more poorly than those from Hamptah Valley, but average ages span a similar Plio-Pleistocene range (Fig. 8): 1.37±0.23 to 3.17±0.71 Ma. The poor reproducibility of these samples is probably attributable to low U contents. Of nineteen individual analyses, ten produced U concentrations less than 3 ppm. Multi-grain AHe ages in samples with such low U contents are susceptible to inaccuracies associated with parent nuclide zonation or U- and/or Th-bearing microinclusions, given that ^{4}He from a small U or Th contamination or spatially heterogeneous ingrown ^{4}He can be a significant contribution to the total helium in an aliquot (House et al., 1997; Farley and Stockli, 2002; Fitzgerald et al., 2006; Reiners and Nicolescu, in press.). Helium produced by the decay of ^{147}Sm may also be relatively significant in such low U samples (Farley and Stockli, 2002). Given that we did not measure ^{147}Sm on the initial runs of these reconnaissance samples, the individual ages for low U samples could thus be too old if ^{147}Sm concentrations were higher than several hundred ppm (Reiners and Nicolescu, in review). An additional complication of low U samples is that, coupled with the young cooling ages, these samples may have ^{4}He contents that are too small to reliably measure. Given ^{4}He blank levels of ~ 0.2 femtomoles (0.0002 pmol), we consider analyses based on less than ~ 0.4 femtomoles to be unreliable (Table 1).

As a result of these problems and the recurring problem of anomalously old ages due to unrecognized inclusions (for example RH2), seven individual age determinations were discarded prior to calculating the mean AHe age from Rohtang Pass and Chattru Valley samples (Table 1). Average age determinations were generally based on only two replicates per sample, and include individual analyses in which the U content was < 3 ppm. Accordingly, we consider all five average ages from this area to be less accurate than the standard deviation of individual replicates. Nevertheless, these data do place a first-order constraint on the cooling history of this region. Based on the resulting average AHe ages, Rohtang Pass and Chattru Valley have experienced similar exhumation rates as the Hamptah Valley since the mid-Pliocene.

4.3 SED data

Our ^{10}Be TCN data are shown in Table 2 and Figs. 9 and 10. Surface exposure ages of individual strath treads from the four locations along the Chandra River range between 5.3±0.5 and 0.2±0.1 ka and rates of fluvial incision calculated as the quotient of the exposure age and height above the river range between 13.2±6.3 and 0.2±0.2 mm/yr. For the one tributary stream of the Chandra that we sampled, surface exposure ages of strath treads range between 2.6±0.3 and 0.9±0.1 ka, and similarly calculated rates of incision range between 12.3±1.9 and 0.6±0.6 mm/a. Our weighted mean rate of incision including all of our data is 2.2±1.2 mm/a. If we exclude the lowest four treads that were 1.5 m or less above the water level when they were collected, the weighted mean rate of incision is 3.5±1.3 mm/a.

For two of the four strath terraces we sampled along the Chandra River there is a correlation between surface height and age (Fig. 10): sample sites CV and KO/ZK yield incision rates of 12 and 5.5 mm/a, respectively. These two incision rates define an envelope that includes data for all of our other sampled locations along the Chandra as well as the tributary stream (location PT).

For locations KL and PT, there is an intermediate-level strath that has a young surface exposure age (Fig. 9) and it is possible that these surfaces (KL1 and PT2) have an unrecognized burial history. Age-height data for straths KL3 and KL2 (Fig. 10) define an incision rate of 1.7 mm/a.

As can be seen in Fig. 9, straths that are all at about the same height do not yield the same age. In addition, not all of the highest tread surfaces yield the oldest ages. The highest strath terrace surface we sampled along the Chandra River, sample CV3 at our easternmost site along the south side of the Chandra is located nearly 20 m above the contemporary river level and yielded an age of 1.6±0.2 ka. Down-river at site KL, sample KL2 located 9 m above the Chandra gave an age of 5.3±0.5 ka, and further down-river just west of Koksar, sample ZK77 located 16 m above the Chandra gave an age of 3.3±0.4 ka.

5. Discussion

5.1 AHe thermochronology

Our AHe ages record recent exhumation of the HHCS in Lahul and fit into the regional pattern of low-temperature thermochronometers in the HHCS yielding Plio-Pleistocene ages (Burbank, et al., 2003; Hodges et al., 2004; Bojar, et al., 2005). Mean AHe ages from the Rohtang Pass and the Chattru Valley are between 1.37±0.23 and 3.17±0.71 Ma, similar to cooling ages for the nearby Ladakh and Garwhal Himalaya (Sorkhabi et al., 1999; Kirstein et al., 2006). Our mean ages from the Rohtang Pass do not define a linear age elevation relationship (AER), nor do the data from the Hamptah Valley (Fig. 8). Over ~ 1 km of vertical relief, ages from the Hamptah Valley vary between 1.39±0.04 and 2.51±0.29 Ma.

The origin of the young cooling ages of Lahul could be two-fold. First, Lahul has been subject to large amounts of glacial and fluvial incision (Owen et al., 2001) and subsequent mass wasting processes. Climate variations associated with the onset of Northern Hemisphere glaciation around 2.7 Ma (Clemens and Tiedemann, 1997) may have increased regional erosion rates in areas such as Lahul that are directly impacted by the monsoon and mid-latitude westerlies (Benn and Owen, 1998). If Lahul straddled the boundary between high monsoon rainfall to the south and arid conditions to the north in Plio-Pleistocene time as it does today (Fig. 3), episodic monsoon-related high rainfall events would have enabled the Chandra and its tributaries to remove accumulated debris from glaciation and mass wasting. Thus, the recent exhumation that Lahul has experienced could be a function of climate change, with the subsequent magnification of erosion rates and the clearing of debris of out this developing mountain topography by fluvial processes. Second, a rapid period of exhumation could be brought about by tectonic uplift. AFT ages between ~ 1.5 and 2.4 Ma similar to our AHe ages have been reported for the Garwhal Himalaya ~ 200 km southeast of Lahul (Sorkhabi et al., 1999). Sorkhabi and others attributed this period of exhumation (~ 2 mm/a) to tectonic uplift and Cenozoic cooling. We cannot be certain of the timing of the onset of exhumation, except to say that it likely predates 2.5 Ma.

Tectonic uplift of the HHCS has been directly linked to models of mid-crustal channel flow and exhumation, and the tectonic evolution of the HHCS is now the archetype for these models. In channel flow, a weak, mid-crustal layer flows laterally between stronger crustal layers above and below, driven by a pressure gradient. At its front, a channel may be simultaneously extruded, that is exhumed by focused surface erosion (see reviews by Godin et al., 2006 and Harris, 2007). Many of the criteria used to predict and identify channel flow have been met by the HHCS, bounded at its base by the MCT and at its top by the STD. Movement along the MCT and STD systems was principally of early to middle Miocene age (summarized by Godin et al., 2006). Hodges (2000) summarized the model of foreland-propagating thrusting as the Himalayan deformation front has progressed from the MCT southward to the Main Boundary thrust in late Miocene-Pliocene and to the Main Frontal thrust in Pliocene-Holocene time. A young, Pliocene to Quaternary phase of exhumation of the HHCS has been supported by patterns of uniform, young AFT and AHe ages across the unit that are spatially related to both thrust and extensional faults (Hurtado et al., 2001; Burbank et al., 2003; Hodges et al., 2004; Vannay et al., 2004; Bojar et al., 2005). Other thermochronologic and thermobarometric studies suggest that the MCT was active as recently as early Pliocene time and records reactivation of hinterland structures or out-of-sequence thrust systems (Macfarlane et al., 1992; Harrison et al., 1997; Catlos et al., 2001, Wobus et al., 2003).

To estimate an exhumation rate in Lahul we assumed a geothermal gradient in the range 25-30°C/km (Vannay et al., 2004; Walker et al., 1999). With this assumption, the AHe closure depth is ~ 3 km, which yields a first-order vertical exhumation rate in the range ~ 1-2 mm/a. Even the most conservative interpretation of our AHe data — using sample RH2-1 and its error (Fig. 8) — yields a first-order exhumation rate of 0.77 mm/a. Calculating “closure-to-surface” exhumation rates is problematic since even for a constant exhumation rate, near-surface isotherms bend beneath topography (Stüwe et al., 1994; Mancktelow and Grasemann, 1997; Ehlers and Farley, 2003) and the rocks may not have been exhumed vertically (Huntington et al., 2007). Changes in surface relief amplitude that have taken place since apatite cooled through its AHe closure temperature have a strong effect on the slope of AERs, with changes in slope affected by topographic wavelength (the horizontal distance between ridge crests), exhumation rate, the geotherm, and the timescale of the change of surface relief (Braun, 2002). Within the limits of our study area, the largest separation of ridge crests is across the Chandra Valley (Fig. 4) where they define a wavelength between ~ 5-8 km; near the lower limit where topographic wavelength significantly affects the bending of isotherms (Mancktelow and Grasemann, 1997; Reiners et al., 2003). Given this small topographic wavelength in our study area and an AHe closure temperature of ~ 70°C, we can conclude that an exhumation rate of ~1-2 mm/a for this part of Lahul is not significantly overestimated.

The youngest mean AHe age we obtained is 1.37±0.23 Ma from the Rohtang Pass. Such young ages suggest that bedrock in our field area was exhumed through cooler, higher crustal levels at the same time or before rocks elsewhere in the HHCS cooled through the higher AFT and ZFT closure temperatures of ~90-120°C and ~ 180-240°C, respectively (Gleadow and Duddy, 1981; Zaun and Wagner, 1985; Reiners and Brandon, 2006). Such local differences in exhumation stand out when compared to the syntaxis (Wadia, 1931) at Nanga Parbat. Zeitler (1985) mapped a contour parallel to the N-S-trending core of Nanga Parbat where ZFT ages were 1.3 Ma or younger. Across the core of Nanga Parbat along the Astor River, ZFT ages are as young as 0.33 Ma (Winslow et al., 1996) and AFT ages are as young as 20 ka (Treloar et al., 2000). At Nanga Parbat, Pleistocene exhumation rates have been estimated to be as high as 3-6 mm/a (Winslow et al., 1994).

5.2 Surface exposure ages of strath terraces

As summarized by Shroder and Bishop (2000), measured rates of fluvial incision should be viewed as an aggregate of sustained erosion and low frequency episodic events (including catastrophic floods). In addition, the storage and mobilization of debris, as well as measurement biases both contribute to the spatial and temporal variation of measured rates. Many different models for the formation of strath terraces have been proposed: response to periods of balanced sediment supply (Formento-Trigilio et al., 2003), altered sediment supply (Pazzaglia and Brandon, 2001; Wegmann and Pazzaglia, 2002), oscillating sediment supply (Hancock and Anderson, 2002), tectonically induced changes in rock uplift (Rockwell et al., 1984; Molnar et al., 1994; Mukul, 1999), falling base level (Born and Ritter, 1970; Reneau, 2000), eustatic sea level fall (Pazzaglia and Gardner, 1993; Merrits et al., 1994), and autocyclic oscillations in erosion rates of meandering channels (Hasbargen and Paola, 2000). However strath terraces are formed, they require that a river incises deeper into its channel (Bucher, 1932) as it abandons its floodplain (Montgomery, 2004). In addition, assuming a consistent river size, greater rates of uplift will produce greater rates of river incision, but without the stream power to erode laterally, the likelihood that strath terraces will be produced or preserved is diminished (Merritts et al., 1994). Physical erosion, too, includes critical thresholds, which suggests that most incision may be propagated by large floods (Whipple, 2004 and references therein). This implies that extreme events, such as glacier outburst floods, and ice- and landslide-dambreak floods may be important factors in the development of strath terraces and long-term incision rates. Lower thresholds, higher precipitation, and steeper, narrower channels permit a higher percentage of floods to contribute to river incision (Tucker, 2004).

Coxon et al. (1996) documented evidence of a past catastrophic flood in the Chandra Valley during the late Quaternary that post-dates the Kulti glacial stage (10–11.4 ka; Owen et al., 2001). This flood was created by the failure of a glacial dam near Batal upstream from our sample locations and left 4-6 m-thick diamicton with imbricated boulders — some with diameters in excess of 10 m — from Batal past the Chattru Valley. The deposits from this catastrophic event are well preserved and overlain by contemporary fan deposits providing evidence that there has been no subsequent large scale flooding. In addition, the presence of avalanche deposits near the banks of the Chandra River provides evidence that seasonal floods do not frequent the Chandra Valley. Therefore, it is likely that there has not been any flooding in the Chandra Valley large enough to leave debris covering the high terrace surfaces we sampled since their abandonment.

In the field, the character and preservation of higher-level strath terrace surfaces suggests that they have not undergone any significant weathering or erosion since their fluvial incision and abandonment but it is possible that intermediate-level surfaces with younger ages (e.g., KL1 and PT2) have an unrecognized burial history (Figs. 9, 10). Of the five strath terraces we sampled, the lowest tread at four of them was only 1.5 m or less above the water level when it was collected (samples KL3, KO1, KON3, and PT3) and these samples are likely to have been submerged at higher water and subject to erosion. Still, their calculated incision rates form an array consistent with the incision envelope of Fig. 10.

Along the Chandra River, the ages of strath terraces higher than 3 m above river level fall between 5.3 and 1 ka. Incision rates calculated for individual strath treads are variable, ranging between 13 and 2 mm/a, but the sets of straths at locations CV and KO/ZK define a more narrow range between 12 and 5.5 mm/a, respectively (Fig. 10). Location CV is farthest upstream, along the south side of the Chandra along a narrow, canyon-like stretch west of Chattru and location KO/ZK is farthest downstream, just west of Koksar. The stretch of the Chandra between these two locations cannot be characterized by a single incision rate but the data suggest some evidence for knickpoint propagation. The tributary slot canyon (location PT) gave incision rates at the higher end of the range for the Chandra: the two higher surfaces yielded rates of 8 and 12 mm/a. It is likely that the lowest PT strath has a burial history.

As with our AHe data, it is informative to compare incision rates in Lahul with those calculated for Himalayan syntaxes. For the Rupal, Buldar and Raikot Rivers which all drain across the Nanga Parbat massif, Shroder and Bishop (2000) reported mean rates of denudation of 25, 7 and 7 mm/a, respectively, and an average incision rate of 22±11 mm/a, based on measurements at 15 sites of fluvial incision of high-elevation glacial terraces along the sides of Nanga Parbat. Leland et al. (1988) calculated bedrock incision rates during the past 7 ka to have been between about 10 and 12 mm/a along the gorge of the Indus River between the Skardu Basin and Nanga Parbat. Perhaps surprisingly, incision rates in Lahul are comparable to these rates at the western syntaxis of the orogen.

5.3 Implications for landscape evolution

Our data allow for a first-order assessment of the state of landscape evolution in Lahul where there has been long-term tectonic rock uplift. As a first estimate, long-term exhumation in Lahul since the Pliocene has been 1-2 mm/a.

Movement along the MCT and STD which bound the HHCS began in the early Miocene. However, along the MCT in Nepal, Hodges et al. (2004) documented Quaternary faulting. Approximately 100 km southeast of Lahul in Sutlej, Vanney et al. (2004) reported AFT ages between 2.7 and 0.9 Ma from the HHCS which record exhumation related to extensional faults, broadly coeval with thrusting in the Lesser Himalayan Crystalline Sequence (LHCS) in the footwall of the MCT. Plio-Pleistocene and Quaternary cooling of the LHCS support a model that as the HHCS channel was exhumed and cooled, its lower bounding thrust propagated towards the foreland and moved to lower structural levels (in the LHCS). The implication of this foreland-propagating thrusting is that faulting along the MCT in the western Himalaya that accommodated the uplift of the HHCS has not persisted in Plio-Pleistocene time, and as a corollary, erosion has not kept pace with the post-Miocene uplift of the HHCS (Beaumont et al., 2001).

If this tectonic scenario is valid, however, we might expect bedrock stream channels in the HHCS to have adjusted to renewed Pleistocene uplift, given response times on the order of 10^6 years (Whipple, 2001) and the effects of orographic precipitation (Fig. 3). The rate of recent, short-term incision along the Chandra River is locally very high, reaching 12 mm/a. This rate is notable, since the Chandra is cutting down through quartzo-feldspathic crystalline bedrock. Bedrock strength (erosivity of bedrock) exerts a critical control on the incision rate of bedrock channels (Riihimaki et al., 2007; Gasparini et al., 2007) and how fast, or whether, a mountain landscape can achieve steady-state. The changing downstream morphology of the Chandra River between Batal and Koksar, and the variability of its incision within this stretch indicate that it is still in post-glacial adjustment to Lahul's tectonically active landscape, where hillslope mass movements appear to be the dominant mechanism of erosion (Owen et al., 1995).

Our calculated incision rates along the Chandra River reflect differential incision over time and the length of the river. There appears to be a lag of ~ 5 ka between the retreat of the main glaciers that reached into the Chandra Valley and fluvial bedrock incision, although it is possible that older, higher terraces have been destroyed or buried by mass wasting events. The age data illustrate the variation that is possible in Himalayan river incision over spatial and temporal scales. This again highlights the varying amounts of incision that are possible over time and space in this active Himalayan environment.

Although our sampling area is relatively small, there is a clear contrast in our incision data with rates and patterns of river incision in other actively uplifting mountains at convergent plate margins that can be interpreted in terms of steady-state landscape evolution (e.g., Pazzaglia and Brandon, 2001). This contrast suggests that Lahul's landscape is in disequilibrium, and given the relatively modest long-term exhumation rate, further suggests that disequilibrium has been persistent on timescales of 10^6 years.

6. Conclusions

Our AHe ages show that exhumation of the HHCS in Lahul from shallow crustal levels to the surface is very young, occurring during the past ~ 2.5 Ma. Even if the uncertainty in our AHe measurements could be reduced — uncertainty largely due to low U concentrations — this conclusion would not change. Our AHe ages also fit into the regional pattern of low-temperature thermochronometers in the HHCS yielding Plio-Pleistocene ages. The largely igneous bedrock in Lahul along the Chandra valley and its tributaries was exhumed from cool, presumably high crustal levels at the same time that rocks in other regions of the HHCS — where there is evidence for active Quaternary faulting and rapid fluvial erosion — were being exhumed from hotter crust where isotherms were likely telescoped near the surface. Surface exposure ages on some strath terraces more than 10 m above the contemporary river level are as ≤1.5 ka. Calculated incision rates along the Chandra are as high as 12-13 mm/a. Thus, on the million-year timescale that typically governs isotope thermochronometers, comparison of AHe ages highlight variations in the near-surface thermal structure of the Himalaya that have developed.

On the millennial timescale recorded by SED, the ages of strath terraces highlight very high fluvial incision throughout the orogen.

Comparison of our AHe and surface exposure ages from Lahul with thermochronometry data from the Nanga Parbat syntaxis illustrates that there are contrasting regions in the High Himalaya where long-term (10^5 – 10^7 years) erosion and exhumation of bedrock substantially differ even though Holocene rates of fluvial incision are comparable, at least locally. These data imply that the orogen's indenting corners are regions where focused denudation has been stable since the mid-Pliocene. Away from these localized areas where there is a potent coupling of tectonic and surface processes that produce rapid uplift and denudation, Plio-Pleistocene erosion and exhumation can be characterized by disequilibrium, where long-term rates are relatively slow and short-term fluvial erosion is highly variable over time and distance.

Acknowledgements

BA would like to thank the Department of Geology at the University of Cincinnati (UC) for providing him with a teaching assistantship that allowed him to undertake this research, Sarah Laxton for all of her support in conducting fieldwork in the unpredictable Indian Himalaya, and funding from the Geological Society of America and Sigma Xi. CD and LAO gratefully acknowledge support for fieldwork from the UC Department of Geology and UC International Programs. Tsewang Dorje provided logistical support in the field and gracious hospitality. Dr. Milap Sharma provided logistical support and equally gracious hospitality in Delhi and Manali. Thanks to Tim Phillips of the UC Department of Geology who helped draft the figures. The manuscript was improved by thorough and thoughtful reviews by Mike Kaplan and an anonymous reviewer.

References

Balco, G., Stone, J.O., Lifton, N.A., Dunai, T.J., 2008. A complete and easily accessible means of calculating surface exposure ages or erosion rates from ^{10}Be and ^{26}Al measurements. Quaternary Geochronology 3, 174-195.

Beaumont, C., Jamieson, R. A., Nguyen, M. H., Lee, B., 2001. Himalayan tectonics explained by extrusion of a low-viscosity crustal channel coupled to focused surface denudation. Nature 414, 738-742.

Benn, D. I., Owen, L. A., 1998. The role of the Indian summer monsoon and the mid-latitude westerlies in Himalayan glaciation; review and speculative discussion. Journal of the Geological Society of London 155, 353-363.

Bojar, A.-V., Fritz, H., Nicolescu, S., Bregar, M., Gupta, R. P., 2005. Timing and mechanisms of Central Himalayan exhumation: discriminating between tectonic and erosion processes. Terra Nova 17, 427-433.

Born, S. M., Ritter, F., 1970. Modern terrace development near Pyramid lake, Nevada, and its geologic implications. Geological Society of America Bulletin 81, 1233-1241.

Bookhagen, B. Burbank, D.W., 2006. Topography, relief, and TRMM-derived rainfall variations along the Himalaya. Geophysical Research Letters 33, L08405, doi:10.1029/2006GL26037.

Braun, J., 2002. Quantifying the effect of recent relief changes on age-elevation relationships. Earth and Planetary Science Letters 200, 331-343.

Braun, J., van der Beek, P., Batt, G., 2006. Quantitative Thermochronology: Numerical Methods for the Interpretation of Thermochronological Data. Cambridge University Press, New York.

Bucher, W. H., 1932. "Strath" as a geomorphic term. Science 75, 130-131.

Burbank, D. W., Anderson, R. S., Brozovic, N., Duncan, C., Fielding, E., Leland, J., Reid, M. R., 1996. Bedrock incision, rock uplift and threshold hillslopes in the northwestern Himalayas. Nature 379, 505-510.

Burbank, D. W., Blythe, A. E., Putkonen, J., Pratt-Sitaula, B., Gabet, E., Oskin, M., Barros, A., Ojha, T. P., 2003. Decoupling of erosion and precipitation in the Himalayas. Nature 426, 652-655.

Catlos, E. J., Grove, M., Harrison, T. M., Kohn, M. J., Manning, C. E., Ryerson, F. J., Upreti, B. N., 2001. Geochronologic and thermobarometric constraints on the evolution of the Main Central Thrust, Central Nepal Himalaya. Journal of Geophysical Research, B, Solid Earth and Planets 106, 16,177-16,204.

Clark, M. K., Royden, L. H., Whipple, K. X., Burchfiel, B. C., Zhang, X., Tang, W., 2006. Use of a regional, relict landscape to measure vertical deformation of the eastern Tibetan Plateau. Journal of Geophysical Research 111, F03002, doi:10.1029/2005JF000294.

Clemens, S. C., Tiedemann, R., 1997. Eccentricity forcing of Pliocene-early Pleistocene climate revealed in a marine oxygen-isotope record. Nature 385, 801-804.

Coxon, P., Owen, L. A., Mitchell, W. A., 1996. A Late Quaternary catastrophic flood in the Lahul Himalayas. Journal of Quaternary Science 11, 495-510.

Cronin, V. S., Johnson, W. P., 1988. Chronostratigraphy of the Late Cenozoic Bunthang sequence and possible mechanism controlling base level in Skardu intermontane basin, Karakoram Himalaya, Pakistan. In: Malinconico, L. L., and Lillie, R. J. (Eds.), Tectonics and Geophysics of the Western Himalayas. Geological Society of America, Denver, CO, pp. 295-309.

Dodson, M. H., 1973. Closure temperature in cooling geochronological and petrological systems. Contributions to Mineralogy and Petrology 40, 259-274.

Dortch, J., Owen, L.A., Haneberg, W.C., Caffee, M.W., Dietsch, C. Kamp, U., 2009. Nature and timing of mega-landslides in northern India. Quaternary Science Reviews, in press.

Ehlers, T. A., Farley, K., 2003. Apatite (U-Th)/He thermochronology: methods and applications to problems in tectonic and surface processes. Earth and Planetary Science Letters 206, 1-14.

Farley, K., Stockli, D. F., 2002. (U-Th)/He dating of phosphates: apatite, monazite, and xenotime. Reviews in Mineralogy and Geochemistry 48, 559-577.

Farley, K. A., 2000. Helium diffusion from apatite: general behavior as illustrated by Durango fluorapatite. Journal of Geophysical Research, B, Solid Earth and Planets 105, 2903-2914.

Fitzgerald, P. G., Baldwin, S. L., Webb, L. E., O'Sullivan, P. B., 2006. Interpretation of (U-Th)/He single grain ages from slowly cooled crustal terranes: A case study from the Transantarctic Mountains of southern Victoria Land. Chemical Geology 225, 91-120.

Formento-Trigilio, M. L., Burbank, D. W., Nicol, A., Rieser, U., Shulmeister, J., 2003. River response to an active fold-and-thrust belt in a convergent margin setting, North Island, New Zealand. Geomorphology 49, 125-152.

Foster, D. A., Gleadow, A. J. W., Mortimer, G., 1994. Rapid Pliocene exhumation in the Karakoram (Pakistan), revealed by fission-track thermochronology of the K2 gneiss. Geology 22, 19-22.

Frank, W., Hoinkes, G., Miller, C., Purtscheller, F., Richter, W., Thoni, M., 1973. Relations between metamorphism and orogeny in a typical section of the Indian Himalayas. Tschermaks Mineralogische und Petrographische Mitteilungen 20, 303-332.

Gasparini, N. M., Bras, R. L., Whipple, K. X., 2007. Predictions of steady state and transient landscape morphology using sediment-flux-dependent river incision models. Journal of Geophysical Research 112, F03S09.

Gleadow, A. J. W., Duddy, I. R., 1981. A natural long-term track annealing experiment for apatite. Nuclear Tracks and Radiation Measurements 5, 169-174.

Godin, L., Grujic, D., Law, R. D., Searle, M. P., 2006. Channel flow, ductile extrusion and exhumation in continental collision zones: an introduction. In: Law, R. D., Searle, M. P., Godin, L. (Eds.), Channel Flow, Ductile Extrusion and Exhumation in Continental Collision Zones. The Geological Society, London, pp. 1-23.

Hancock, G. S., Anderson, S., 2002. Numerical modeling of fluvial strath-terrace formation in response to oscillating climate. Geological Society of America Bulletin 114, 1131-1142.

Harris, N., 2007. Channel flow and the Himalayan-Tibetan orogen: a critical review. Journal of the Geological Society 164, 511-523.

Harrison, T. M., Lovera, O. M., Grove, M., 1997. New insights into the origin of two constrasting Himalayan granite belts. Geology 25, 899-902.

Hasbargen, L. E., Paola, C., 2000. Landscape instability in an experimental drainage basin. Geology 28, 1067-1070.

Hodges, K. V., 2000. Tectonics of the Himalaya and southern Tibet from two perspectives. Geological Society of America Bulletin 112, 324-350.

Hodges, K.V., 2006. A synthesis of the channel flow-extrusion hypothesis as developed for the Himalaya-Tibetan orogenic system. In: Law, R. D., Searle, M. P., Godin, L. (Eds.), Channel Flow, Ductile Extrusion and Exhumation in Continental Collision Zones. The Geological Society, London, pp. 71-90.

Hodges, K. V., Wobus, C., Ruhl, K., Schildgen, T., Whipple, K., 2004. Quarternary deformation, river steepening, and heavy precipitation at the front of the Higher Himalayan ranges. Earth and Planetary Science Letters 220, 379-389.

House, M. A., Wernicke, B., Farley, K., Dumitru, T. A., 1997. Cenozoic thermal evolution of the central Sierra Nevada from (U-Th)/He thermochronometry. Earth and Planetary Science Letters 151, 167-179.

Huntington, K. W., Ehlers, T. A., Hodges, K. V., Whipp, D. M., Jr., 2007. Topography, exhumation pathway, age uncertainties, and the interpretation of thermochronometer data. Tectonics 26, TC4012, doi:10.1029/2007/TC002108.

Hurtado, J. M., Jr., Hodges, K. V., Whipple, K., 2001. Neotectonics of the Thakkhola Graben and implications for Recent activity on the South Tibetan fault system in the central Nepal Himalaya. Geological Society of America Bulletin 113, 222-240.

Kirby, E., Reiners, P. W., Krol, M. A., Whipple, K. X., Hodges, K. V., Farley, K. A., Tang, W., Chen, Z., 2002. Late Cenozoic evolution of the eastern margin of the Tibetan Plateau: Inferences from $^{40}Ar/^{39}Ar$ and (U-Th)/He thermochronology. Tectonics 21, doi:10.1029/2000TC001246.

Kirstein, L. A., Dobson, K., Sinclair, H., Stuart, F. M., 2006. Rapid early Miocene exhumation of the Ladakh Batholith, western Himlalayas. Geology 34, 1049-1052.

Lal, D., 1991. Cosmic ray labeling of erosion models. Earth and Planetary Science Letters 104, 429-439.

Lamb, S., Hoke, L., Kennan, L., Dewey, J. F., 1997. Cenozoic evolution of the Central Andes in Bolivia and northern Chile. In: Burg, J.-P., Ford, M. (Eds.), Orogeny Through Time. The Geological Society, London, pp. 237-264.

Leland, J., Reid, M. R., Burbank, D., Finkel, R., Caffee, M., 1998. Incision and differential bedrock uplift along the Indus River near Nanga Parbat, Pakistan Himalaya, from ^{10}Be and ^{26}Al exposure age dating of bedrock straths. Earth and Planetary Science Letters 154, 93-107.

Lister, G. S., Forster, M. A., Rawling, T. J., 2001. Episodicity during orogenesis. In: Miller, J. A., Holdsworth, R. E., Buick, I. S., Hand, M. (Eds.), Continental Reactivation and Reworking. The Geological Society, London, pp. 89-113.

Macfarlane, A., Hodges, K. V., Lux, D., 1992. A structural analysis of the Main Central thrust zone, Langtang National Park, central Nepal Himalaya. Geological Society of America Bulletin 104, 1389–1402.

Mancktelow, N. S., Grasemann, B., 1997. Time-dependent effects of heat advection and topography on cooling histories during erosion. Tectonophysics 270, 167-195.

McDowell, F. W., McIntosh, W. C., Farley, K. A., 2005. A precise $^{40}Ar/^{39}Ar$ reference age for the Durango apatite (U-Th)/He and fission track dating standard. Chemical Geology 214, 249-263.

Merritts, D. J., Vincent, K. R., Wohl, E. E., 1994. Long river profiles, tectonism, and eustasy: a guide to interpreting fluvial terraces. Journal of Geophysical Research 99, 14,031-14,050.

Miller, C., Thoni, M., Frank, W., Grasemann, B., Klotzli, U., Guntli, P., Draganits, E., 2001. The early Palaeozoic magmatic event in the Northwest Himalaya, India: source, tectonic setting and age of emplacement. Geological Magazine 138, 237-251.

Molnar, P., Brown, E. T., Burchfiel, B. C., Deng, Q., Feng, X., Li, J., Raisbeck, G. M., Shi, J., Wu, Z., Yiou, F., You, H., 1994. Quaternary climate change and the formation of river terraces across growing anticlines on the north flank of the Tien Shan, China. Journal of Geology 102, 583-602.

Montgomery, D. R., 2004. Observations on the role of lithology in strath terrace formation and bedrock channel width. American Journal of Science 304, 454-476.

Mukul, M., 1999. The geometry and kinematics of the Main Boundary Thrust and related neotectonics in the Darjiling Himalayan fold-and-thrust belt, West Bengal, India. Journal of Structural Geology 22, 1261-1283.

Nishiizumi, K., Winterer, E. L., Kohl, C. P., Klein, J., Middleton, R., Lal, D., Arnold, J. R., 1989. Cosmic ray production of ^{10}Be and ^{26}Al in quartz from glacially polished rocks. Journal of Geophysical Research 94, 17,907-17,915.

Owen, L. A., Benn, D. I., Derbyshire, E., Evans, D. J. A., Mitchell, W. A., Thompson, D., Richardson, S., Lloyd, M., Holden, C., 1995. The geomorphology and landscape evolution of the Lahul Himalaya, Northern India. Z. Geomorph. N.E. 39, 145-174.

Owen, L. A., Bailey, R. M., Rhodes, E. J., Mitchell, W. A., Coxon, P., 1997. Style and timing of glaciation in the Lahul Himalaya, northern India: a framework for reconstructing late

Quaternary palaeoclimatic change in the western Himalayas. Journal of Quaternary Science 12, 83-109.

Owen, L. A., Benn, D. I., Caffee, M. W., Finkel, R. C., Gualtieri, L., Sharma, M. C., 2001. Cosmogenic radionuclide dating of glacial landforms in the Lahul Himalaya, northern India; defining the timing of late Quaternary glaciation. Journal of Quaternary Science 16, 555-563.

Owen, L. A., Finkel, R. C., Caffee, M. W., Gualtieri, L., 2002. Timing of multiple glaciations during the Late Quaternary in the Hunza Valley, Karakoram Mountains, Northern Pakistan: defined by cosmogenic radionuclide dating of moraines. Geological Society of America Bulletin 114, 593-604.

Owen, L. A., Bovard, K. R., Caffee, M. W., Finkel, R. C., Sharma, M. C., 2006. Terrestrial cosmogenic nuclide surface exposure dating of the oldest glacial successions in the Himalayan Orogen; Ladakh Range, northern India. Geological Society of America Bulletin 118, 383-392.

Owen, L.A., Caffee, M.W., Finkel, R.C. Seong, B.Y., 2008. Quaternary glaciations of the Himalayan-Tibetan orogen. Journal of Quaternary Science 23, 513-532.

Pazzaglia, F. J., Brandon, M. T., 2001. A fluvial record of long term steady-state uplift and erosion across the Cascadia forearc high, western Washington State. American Journal of Science 301, 385-431.

Pazzaglia, F. J., Gardner, W., 1993. Fluvial terraces of the lower Susquehanna River. Geomorphology 8, 83-113.

Quarles van Ufford, A., Cloos, M., 2005. Cenozoic tectonics of New Guinea. AAPG Bulletin 89, 119-140.

Reiners, P. W., Brandon, M. T., 2006. Using thermochronology to understand orogenic erosion. Annual Review of Earth and Planetary Science 34, 419-466.

Reiners, P.W., Nicolescu, S., *in press*. Measurement of parent nuclides for (U-Th)/He chronometry by solution sector ICP-MS. Geochimica Cosmochimica Acta.

Reiners, P. W., Zhou, Z., Ehlers, T. A., Xu, C., Brandon, M., Donelick, R. A., Nicolescu, S., 2003. Post-orogenic evolution of the Dabie Shan, eastern China, from (U-Th)/He and fission-track thermochronology. American Journal of Science 303, 489-518.

Reneau, S. L., 2000. Stream incision and terrace development in Frijoles Canyon, Bandelier National Monument, New Mexico, and the influence of lithology and climate. Geomorphology 32, 171-193.

Riihimaki, C. A., Anderson, R. S., Safran, E. B., 2007. Impact of rock uplift on rates of late Cenozoic Rocky Mountain river incision. Journal of Geophysical Research 112, F03S02.

Rockwell, T. K., Clark, M. N., Johnson, D. L., Keller, E. A., 1984. Chronology and rates of faulting of Ventura River terraces, California. Geological Society of America Bulletin 95, 1466-1474.

Searle, M. P., 1991. Geology and Tectonics of the Karakoram Mountains. J. Wiley and Sons, Chichester.

Searle, M. P., Fryer, B. J., 1986. Garnet and muscovite-bearing leucogranites, gneisses, and migmatites of the Higher Himalaya from Zanskar, Kulu, Lahoul, and Kashmir. Collision Tectonics 19, 185-201.

Shroder, J. F., Bishop, M. P., 2000. Unroofing of the Nanga Parbat Himalaya. In: Khan, M. A., Treloar, P. J., Searle, M. P., Jan, M. Q. (Eds.), Tectonics of the Nanga Parbat Syntaxis and the Western Himalaya. The Geological Society, London, pp. 163-179.

Sorkhabi, R. B., Foland, K. A., Jain, A. K., Manickavasagam, R. M., 1999. Tectonic and cooling history of the Garhwal Higher Himalaya, Bhagirathi Valley: constraints from thermochronological data. Gondwana Research Group Memoir 6, 217-235.

Steck, A., Bucher, H., Marchant, R., Masson, H., Spring, L., Stutz, E., 1993. Geological transect across the northwestern Himalaya in eastern Ladakh and Lahul (a model for the continental collision of India and Asia). Eclogae Geologicae Helvetiae 86, 219-263.

Stone, J. O., 2000. Air pressure and cosmogenic isotope production. Journal of Geophysical Research 105, 23753-23759.

Stuwe, K., Brown, R., White, L., 1994. The influence of eroding topography on steady-state isotherms: application tot fission track analysis. Earth and Planetary Science Letters 124, 63-74.

Treloar, P. J., Rex, D. C., Guise, P. G., Wheeler, J., Hurford, A. J., Carter, A., 2000. Geochronological constraints on the evolution of the Nanga Parbat syntaxis, Pakistan Himalaya. In: Khan, M. A., Treloar, P. J., Searle, M. P., Jan, M. Q. (Eds.), Tectonics of the Nanga Parbat Syntaxis and the Western Himalaya. The Geological Society, London, pp. 137-162.

Tucker, G. E., 2004. Drainage basin sensitivity to tectonic and climatic forcing: implications of a stochastic model for the role of entrainment and erosion thresholds. Earth Surface Processes and Landforms 29, 185-205.

Vannay, J.-C., Grasemann, B., Rahn, M., Frank, W., Carter, A., Baudraz, V., Cosca, M., 2004. Miocene to Holocene exhumation of metamorphic crustal wedges in the NW Himalaya: Evidence for tectonic extrusion coupled to fluvial erosion. Tectonics 23, TC1014, p. doi:10.1029/2002TC001429.

Vannay, J.-C., Steck, A., 1995. Tectonic evoluiton of the High Himalaya in Upper Lahul (NW Himalaya, India). Tectonics 14, 253-263.

Wadia, D. N., 1931. The syntaxis of the northwest Himalaya: its rocks, tectonics and orogeny. Rec. Geol. Surv. India 65.

Walker, J. D., Martin, M. W., Bowring, S. A., Searle, M. P., Waters, D. J., Hodges, K. V., 1999. Metamorphism, melting, and extension: Age constraints from the High Himalayan slab of southeast Zanskar and northwest Lahul. The Journal of Geology 107, 473-495.

Webb, A. A. G., Yin, A., Harrison, T. M., Celerier, J., Burgess, W. P., 2007. The leading edge of the Greater Himalaya Crystalline complex revealed in the NW Indian Himalaya: Implications for the evolution of the Himalayan orogen. Geology 35, 955-958.

Wegmann, K. W., Pazzaglia, J., 2002. Holocene strath terraces, climate change, and active tectonics; the Clearwater River basin, Olympic Peninsula, Washington State. Geological Society of America Bulletin 114, 731-744.

Whipple, K. X., 2001. Fluvial landscape response time: How plausible is steady-state denudation? American Journal of Science 301, 313-325.

Whipple, K.X., 2004. Bedrock rivers and the geomorphology of active orogens: Annual Reviews of Earth and Planetary Sciences 32, 151-185.

Winslow, D. M., Chamberlain, C. P., Williams, I. S., Zeitler, P. K., 1996. Geochronologic constraints on syntaxial development in the Nanga Parbat region, Pakistan. Tectonics 15, 1292-1308.

Winslow, D. M., Zeitler, P. K., Chamberlain, C. P., Hollister, L. S., 1994. Direct evidence for a steep geotherm under conditions of rapid denudation, Western Himalaya, Pakistan. Geology 22, 1075-1078.

Wobus, C. W., Hodges, K. V., Whipple, K. X., 2003. Has focused denudation sustained active thrusting at the Himalayan topographic front? Geology 31, 861-864.

Wolf, R. A., Farley, K. A., Silver, L. T., 1996. Helium diffusion and low-temperature thermochronology of apatite. Geochimica et Cosmochimica Acta 60, 4231-4240.

Wyss, M., Hermann, J., Steck, A., 1999. Structural and metamorphic evolution of the northern Himachal Himalaya, NW India (Spiti - eastern Lahul - Parvati valley traverse). Eclogae Geologicae Helvetiae 92, 3-44.

Zaun, P. E., Wagner, G. A., 1985. Fission-track stability in zircons under geological conditions. Nuclear Tracks and Radiation Measurements 10, 303-307.

Zeitler, P. K., 1985. Cooling history of the NW Himalaya Pakistan. Tectonics 4, 127-151.

Zeitler, P. K., Herczig, A. L., McGougall, I., Honda, M., 1987. U-Th-He dating of apatite: a potential thermochronometer. Geochimica et Cosmochimica Acta 51, 2865-2868.

Zeitler, P. K., Meltzer, A. S., Koons, P. O., Craw, D., Hallet, B., Chamberlain, C. P., Kidd, W. S. F., Park, S. K., Seeber, L., Bishop, M., Shroder, J., 2001. Erosion, Himalayan geodynamics, and the geomorphology of metamorphism. GSA Today 11, 4-9.

Figures

Fig. 1. Regional location of the field area (red square) and ASTER satellite imagery of the Lahul region. Areas of interest where samples for AHe and TCN geochronology were collected are outlined in varying colors.

Fig. 2. Geologic map of the study area (simplified from Webb et al., 2007). Contact marked by square tic marks is the South Tibetan detachment fault, which places rocks of the Tethyan

Himalayan sequence in contact with rocks of the HHCS. Small bodies of leucogranite in the HHCS are omitted for clarity.

Fig. 3. Calibrated Tropical Rainfall Measurement Mission (TRMM)-based monsoon rainfall amounts averaged from satellite data collected 2 to 4 times daily from January 1998 to December 2005. The satellite data comprise instantaneous rainfall measurement with a spatial resolution of ~ 5 x 5 km (modified from Bookhagen and Burbank, 2006).

Fig. 4. Shaded relief image produced using a 30 m ASTER digital elevation model of the study area and topographic profiles drawn perpendicular to the Chandra Valley. Profile locations are shown on the shaded relief image. Dashed lines on the profiles indicate the four terrace levels described in the text.

Fig. 5. Sampling sites for AHe and TCN analyses. Green circles denote the locations of sampled bedrock for AHe thermochronometry and yellow circles denote the location of sampled strath terraces; latitude and longitude coordinates and elevations are given in Tables 1 and 2, respectively. AHe samples are from the Hamptah Valley (HA), Rohtang Pass (RH), and Chattru Valley (CH). TNC samples (from east to west) are from the south side of the Chandra River (CV), the base of an unnamed tributary stream on the north side of the Chandra (PT), just east of the Kulti Valley on the north side of the Chandra (KL), and just west of Koksar on the south side of the Chandra (KON and ZK).

Fig. 6. Field photos of Lahul landscape, including AHe sampling sites. (A) Bedrock exposure near the Rohtang Pass (AHe samples RH1 and RH2). (B) Looking north up the Chattru Valley (AHe samples CH-1) from the Hamptah Valley. (C) Looking south from within the Kulti

Valley. Note sandur in the foreground. (D) Looking south to the Hamptah Pass (AHe samples HA) from high in the Chattru Valley. (E) The southern wall of the Chandra Valley. An oblique view of the mouth of the Hamptah Valley can be seen in the middle of the photo. The vast majority of this southern wall is composed of leucogranite.

Fig. 7. Examples of strath terrace TCN sampling sites. (A) Tributary stream of the Chandra River. Terraces found on top of and within this slot canyon were sampled (samples PT1-PT3). (B) Strath terraces just to the east of the Kulti Valley, on the north side of the Chandra River (samples KL1-KL3). (C) Terraces are located just west of Koksar on the south side of the Chandra River (samples KO1-KO3). (D) Terraces located east of Koksar, on the north side of the Chandra River (KON2 and KON3). Koksar can be seen in the background. (E) Easternmost sampled strath terraces located on the south side of the Chandra River (samples CV1-CV3). Distortion of the stitched photos make the river appear to bend; this is not a true feature.

Fig. 8 AHe age-elevation data. Error bars are the standard deviation of the mean sample cooling age. AHe ages from the Hamptah Valley show no correlation between age and elevation.

Fig. 9. Schematic profiles of strath terraces and TCN surface exposure ages.

Fig. 10. TCN ages of strath terraces along the Chandra River and one of its tributaries (PT) *vs.* their measured heights above the river level; sample locations are given in Figure 5. Error bars are from Table 2. Linear trendlines are fitted to the straths at location CV and downstream, location KO, ZK yielding incision rates of 12 and 5.5 mm/a, respectively. The trendlines define an incision envelope that includes data from the KL, KON, and PT locations. Low straths near

the river level systematically record progressively higher incision rates consistent with the incision envelope. The two KL data with the oldest ages likely have complex burial histories and inherited ^{10}Be.

Figure 1


Koksar
Greater Himalaya
Batal
Pir Panjal
Pakistan
China
India
Nepal
10 km
Chandra River
Rohtang Pass
Kulti Valley
Chattru Valley
Hamptah Valley
N

Figure 2

Figure 2

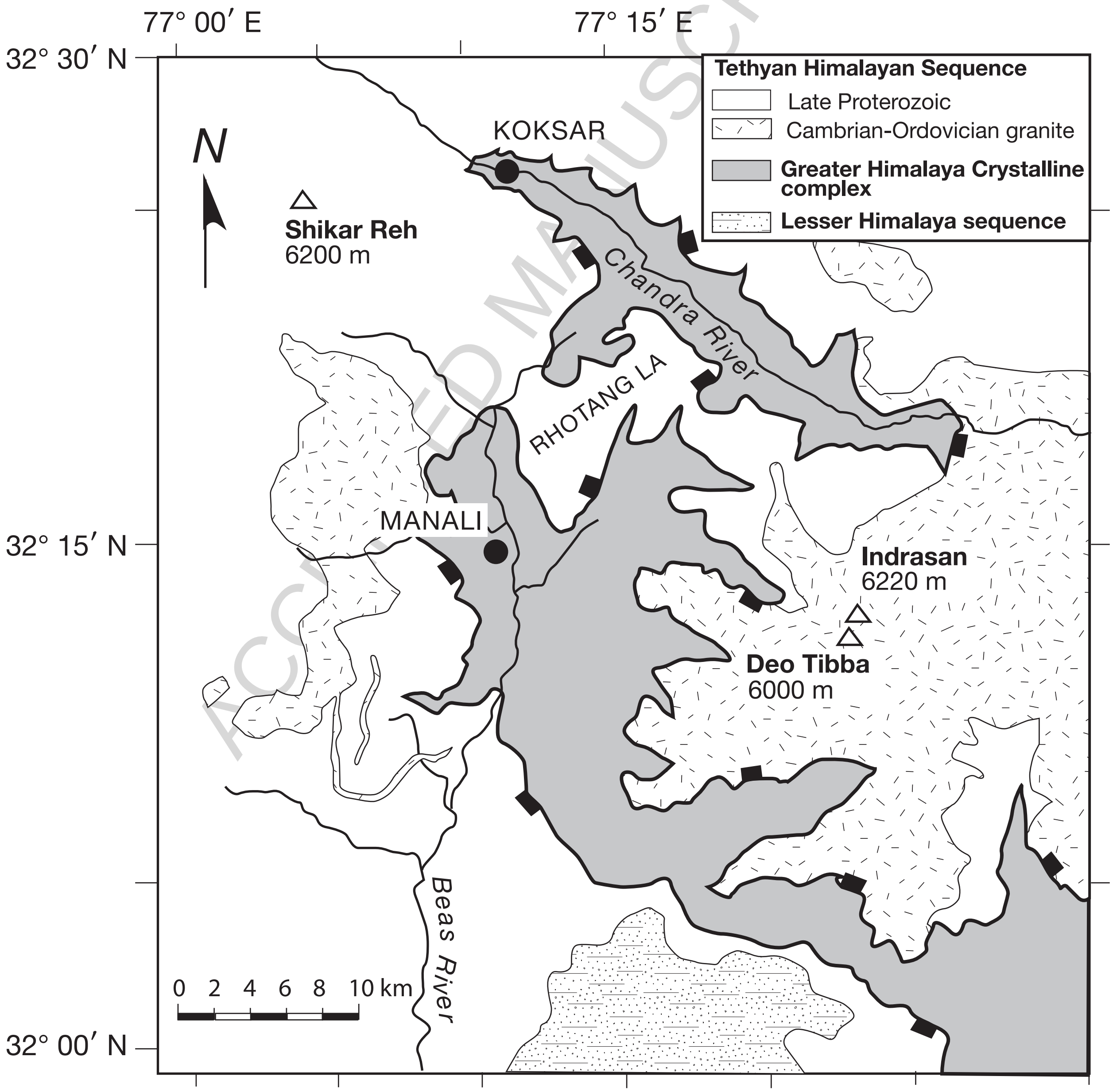

Figure 3

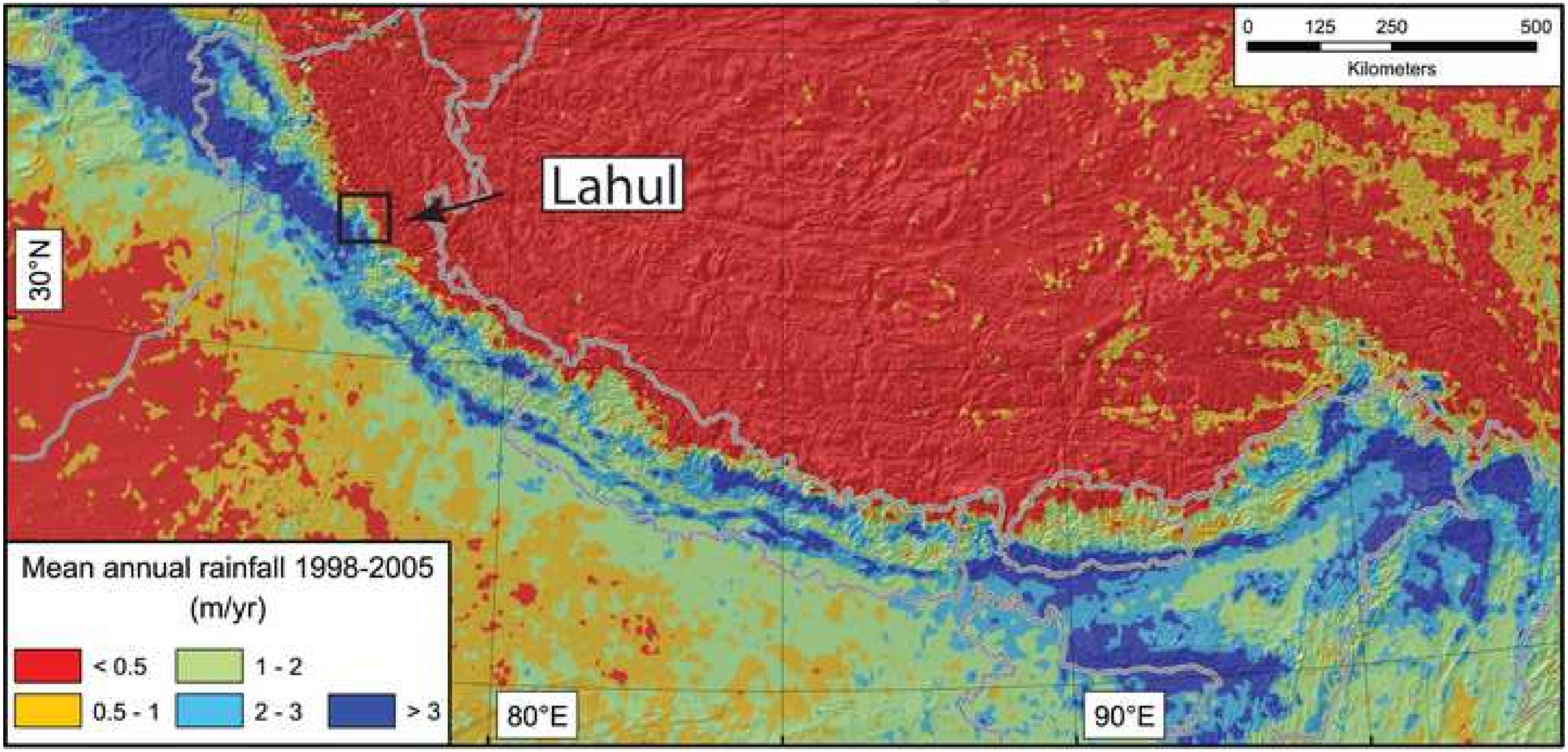

0
125
250
500
Kilometers
Lahul
30°N
Mean annual rainfall 1998-2005 (m/yr)
< 0.5
1 - 2
0.5 - 1
2 - 3
> 3
80°E
90°E

Figure 4

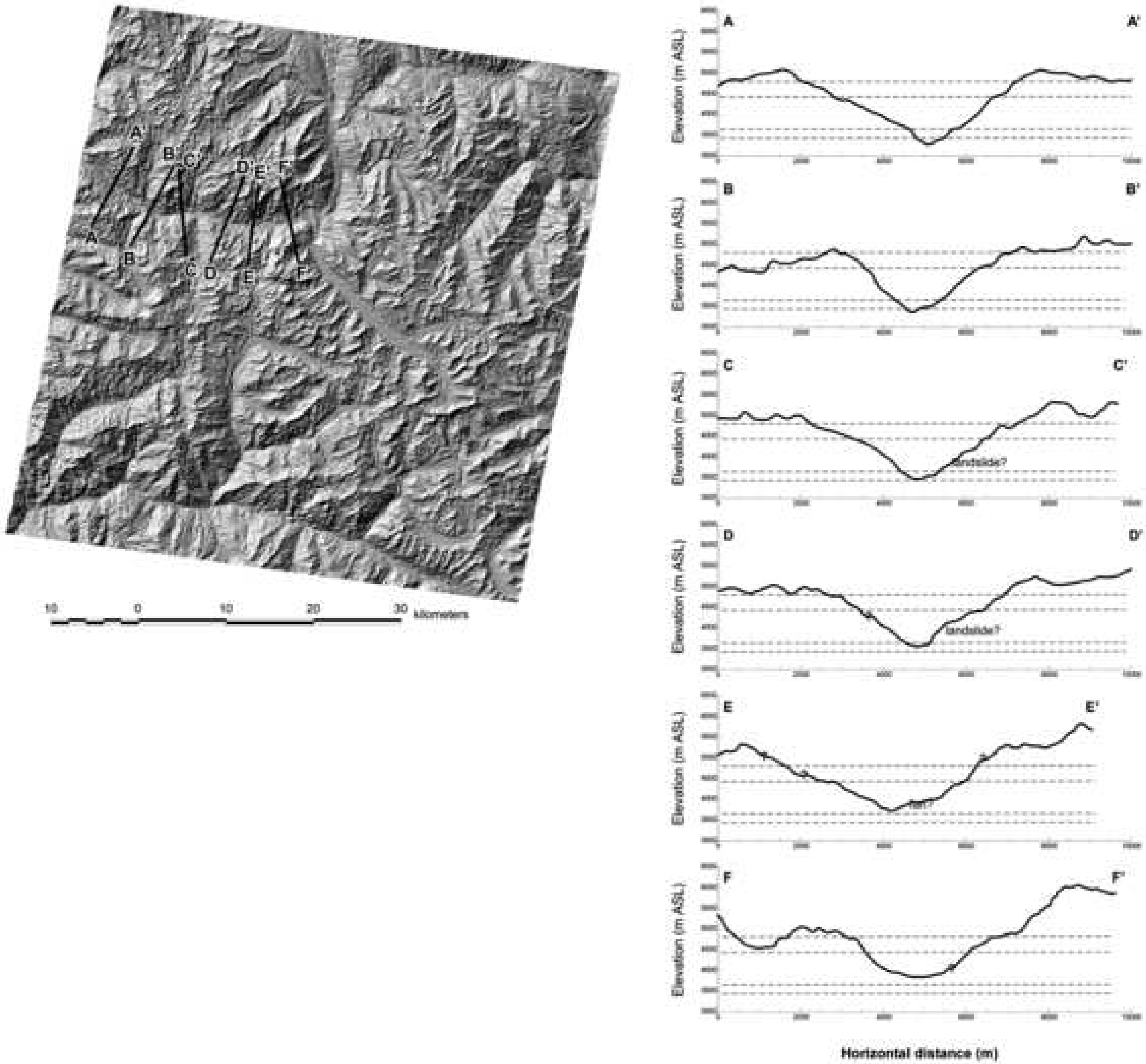
A
A'
B
B'
C
C'
D
D'
E
E'
F
F'
10
0
10
20
30
kilometers
Elevation (m ASL)
landslide?
fan?
Horizontal distance (m)

Figure 5

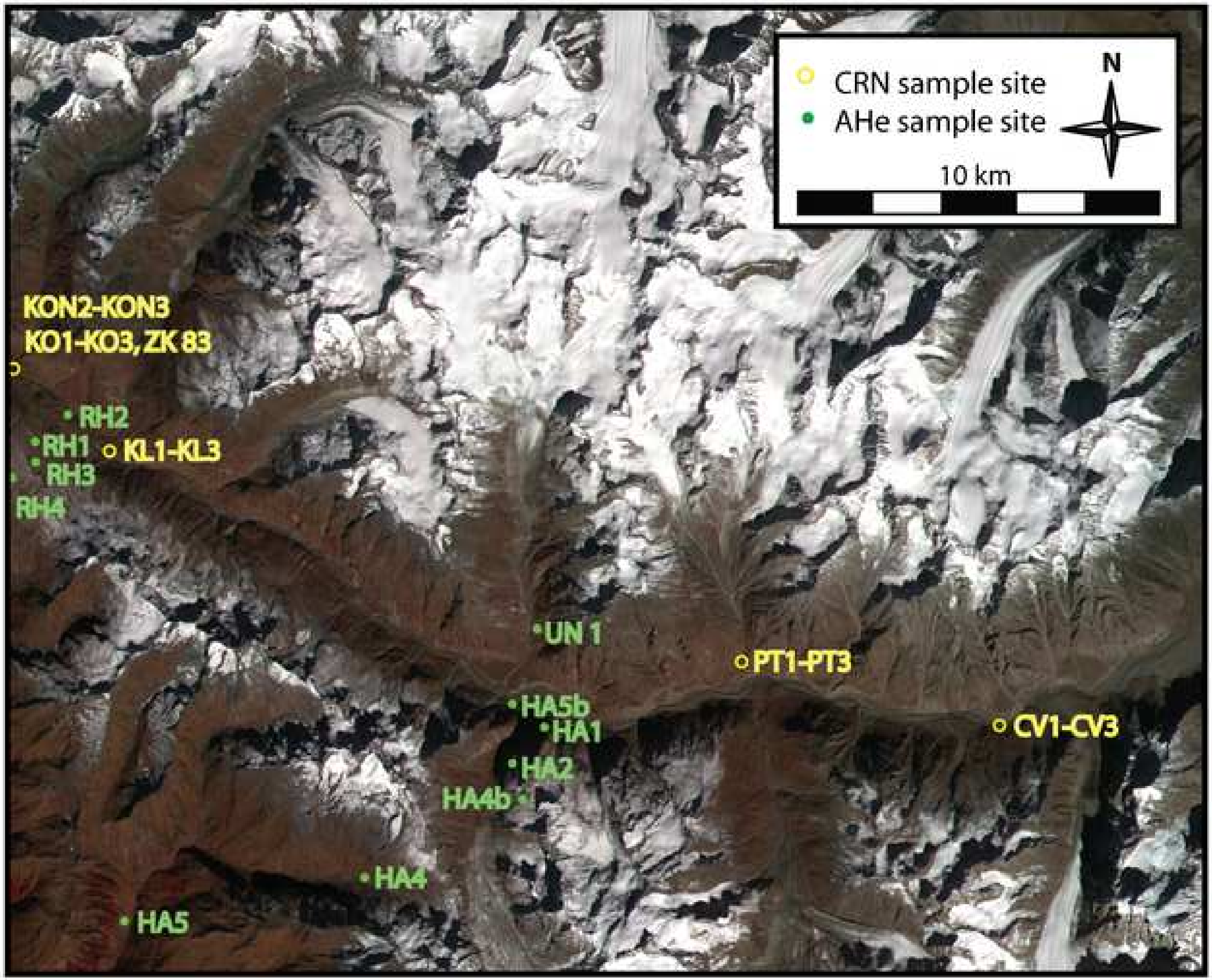
CRN sample site
AHe sample site
N
10 km
KON2-KON3
KO1-KO3, ZK 83
RH2
RH1
KL1-KL3
RH3
RH4
UN 1
PT1-PT3
HA5b
HA1
CV1-CV3
HA2
HA4b
HA4
HA5

Figure 6

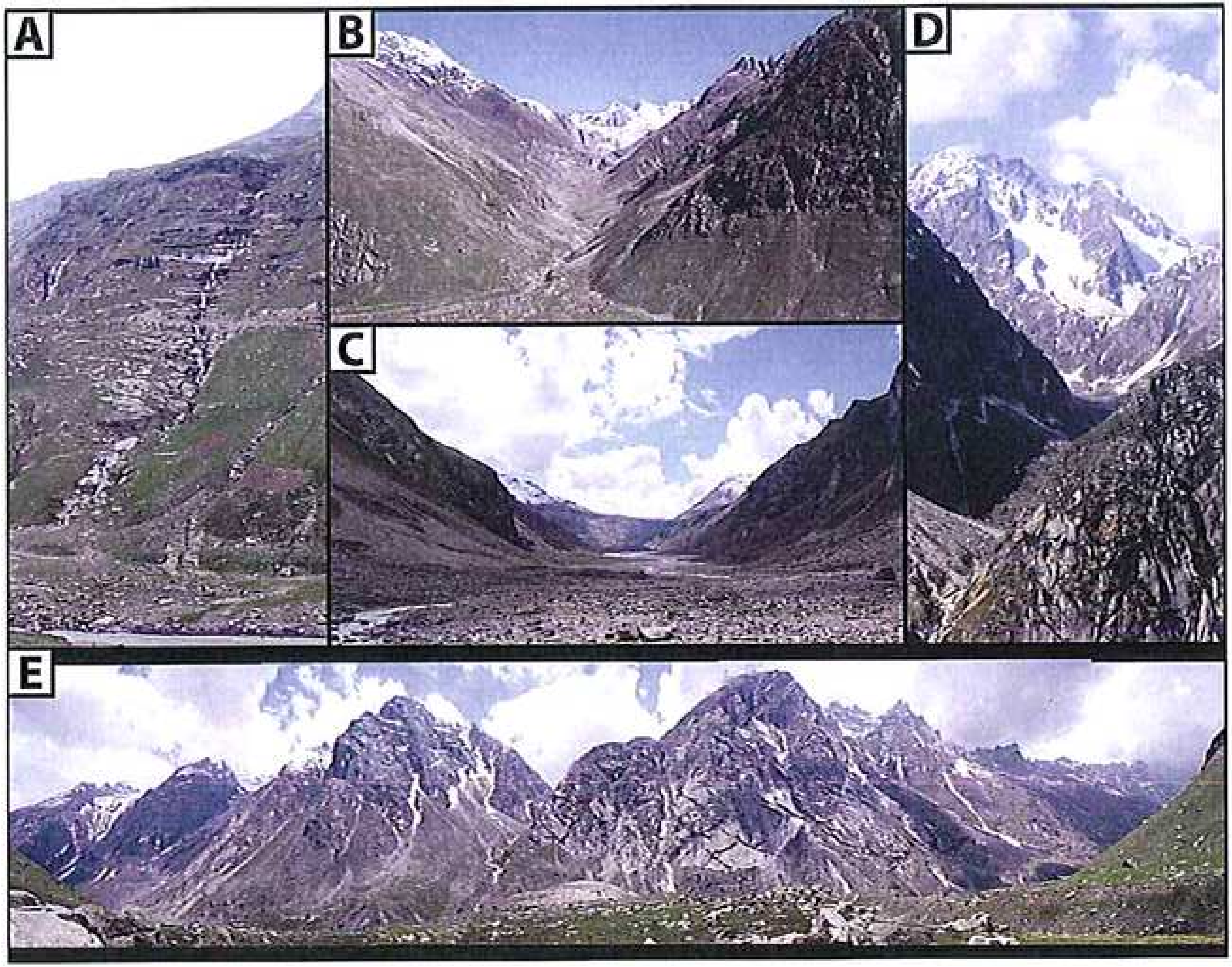

Figure 7

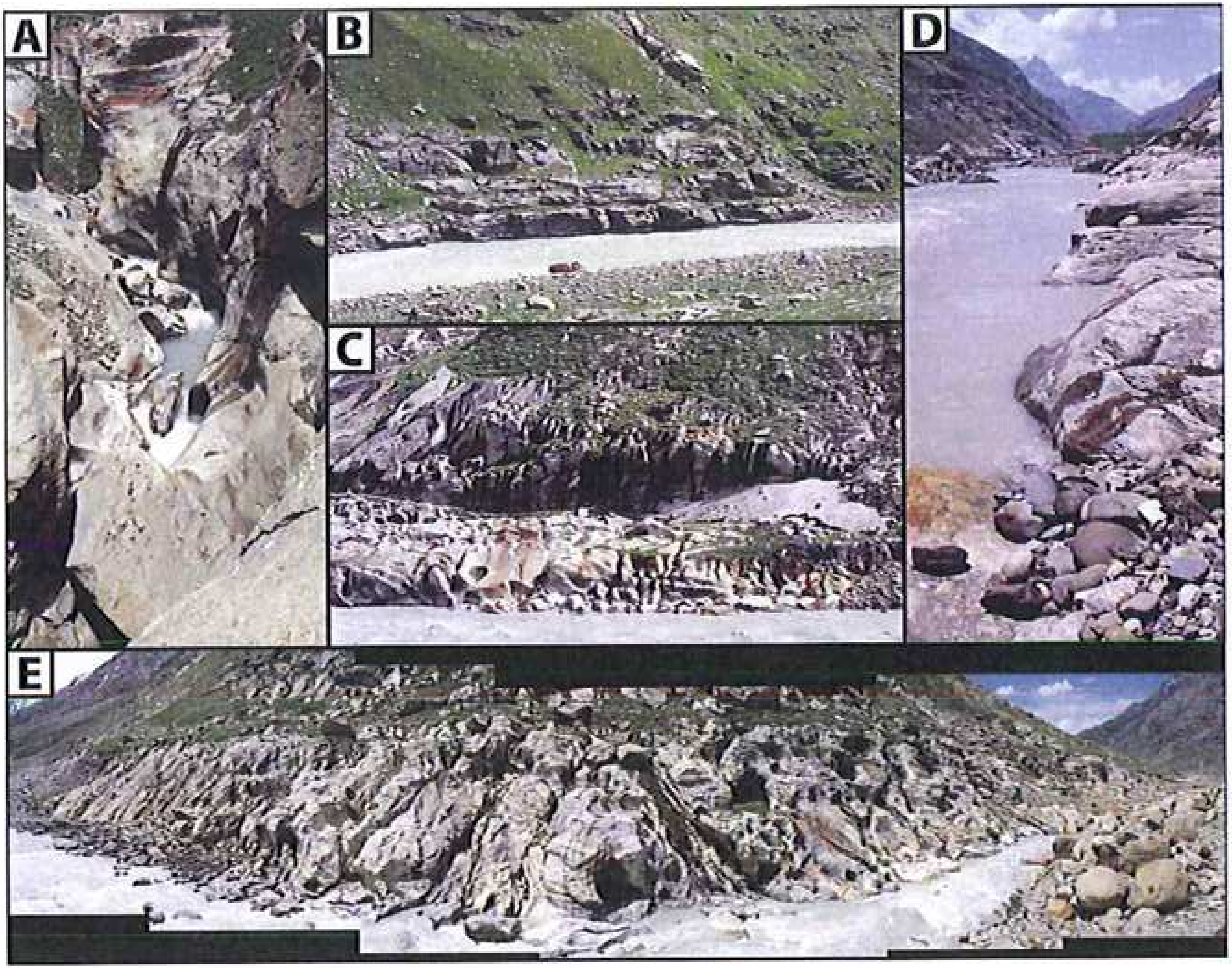

Figure 8

Figure 8

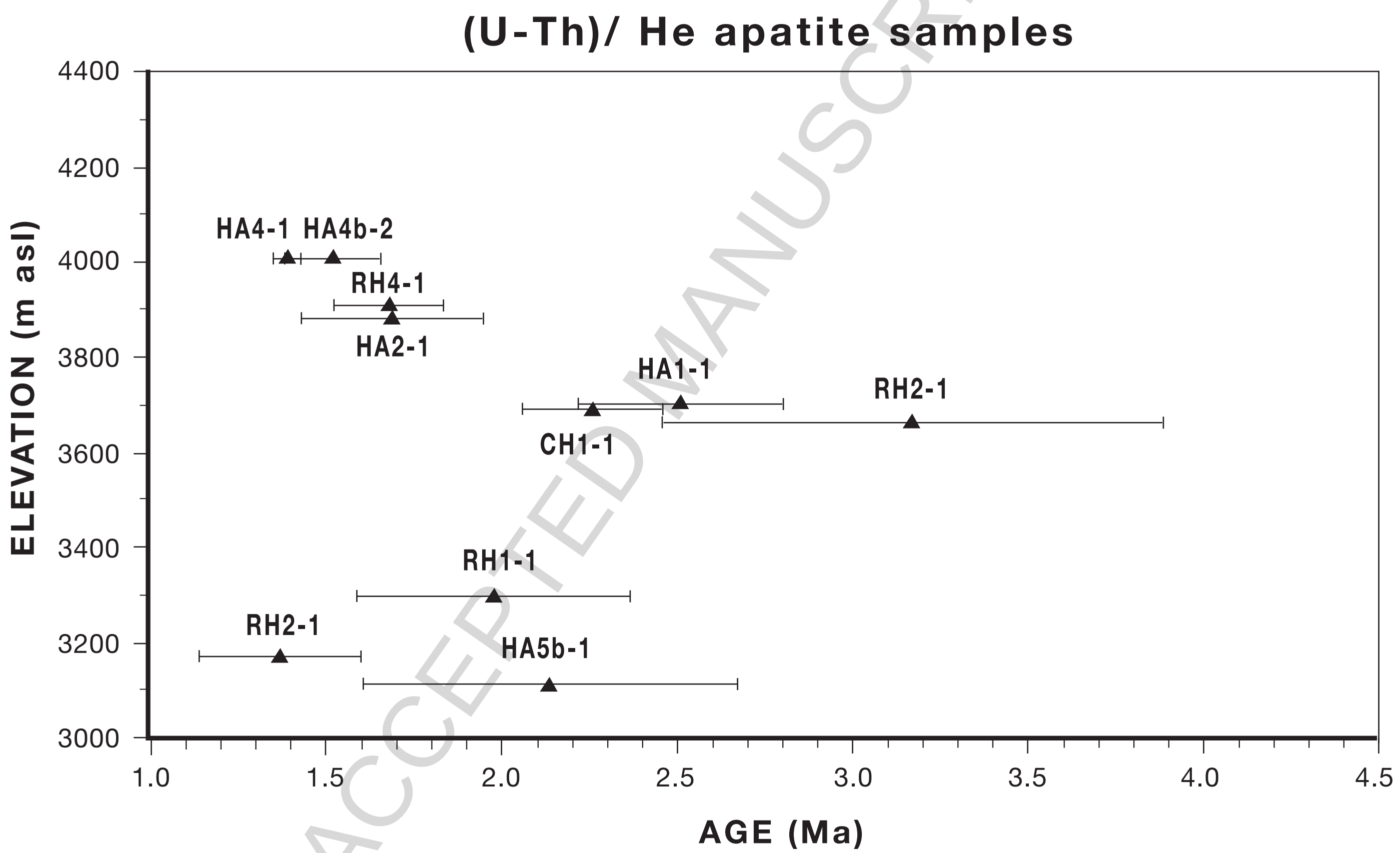

Figure 9

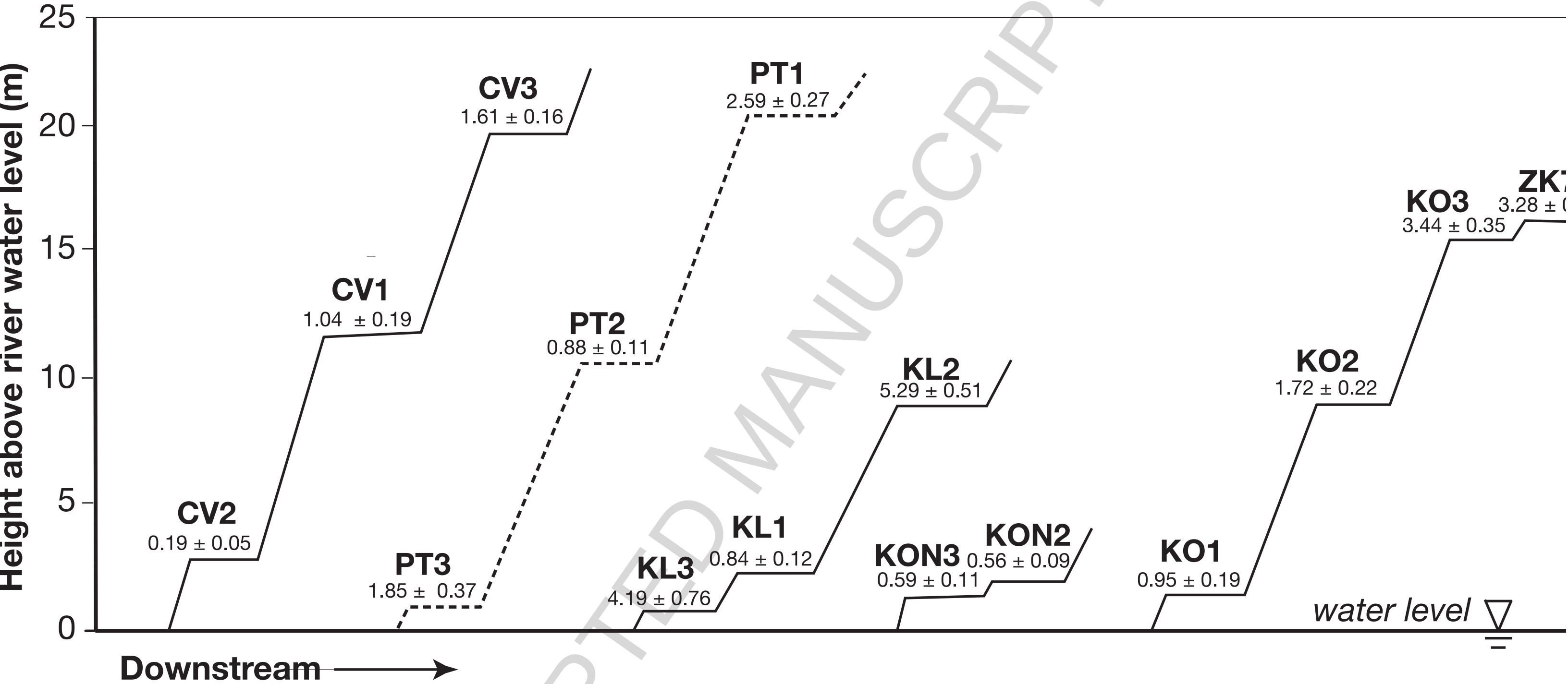

Height above river water level (m)
25
20
15
10
5
0
CV2
0.19 ± 0.05
CV1
1.04 ± 0.19
CV3
1.61 ± 0.16
PT3
1.85 ± 0.37
PT2
0.88 ± 0.11
PT1
2.59 ± 0.27
KL3
4.19 ± 0.76
KL1
0.84 ± 0.12
KL2
5.29 ± 0.51
KON3
0.59 ± 0.11
KON2
0.56 ± 0.09
KO1
0.95 ± 0.19
KO2
1.72 ± 0.22
KO3
3.44 ± 0.35
ZK7
3.28 ±
water level
Downstream

Figure 10

Figure 10

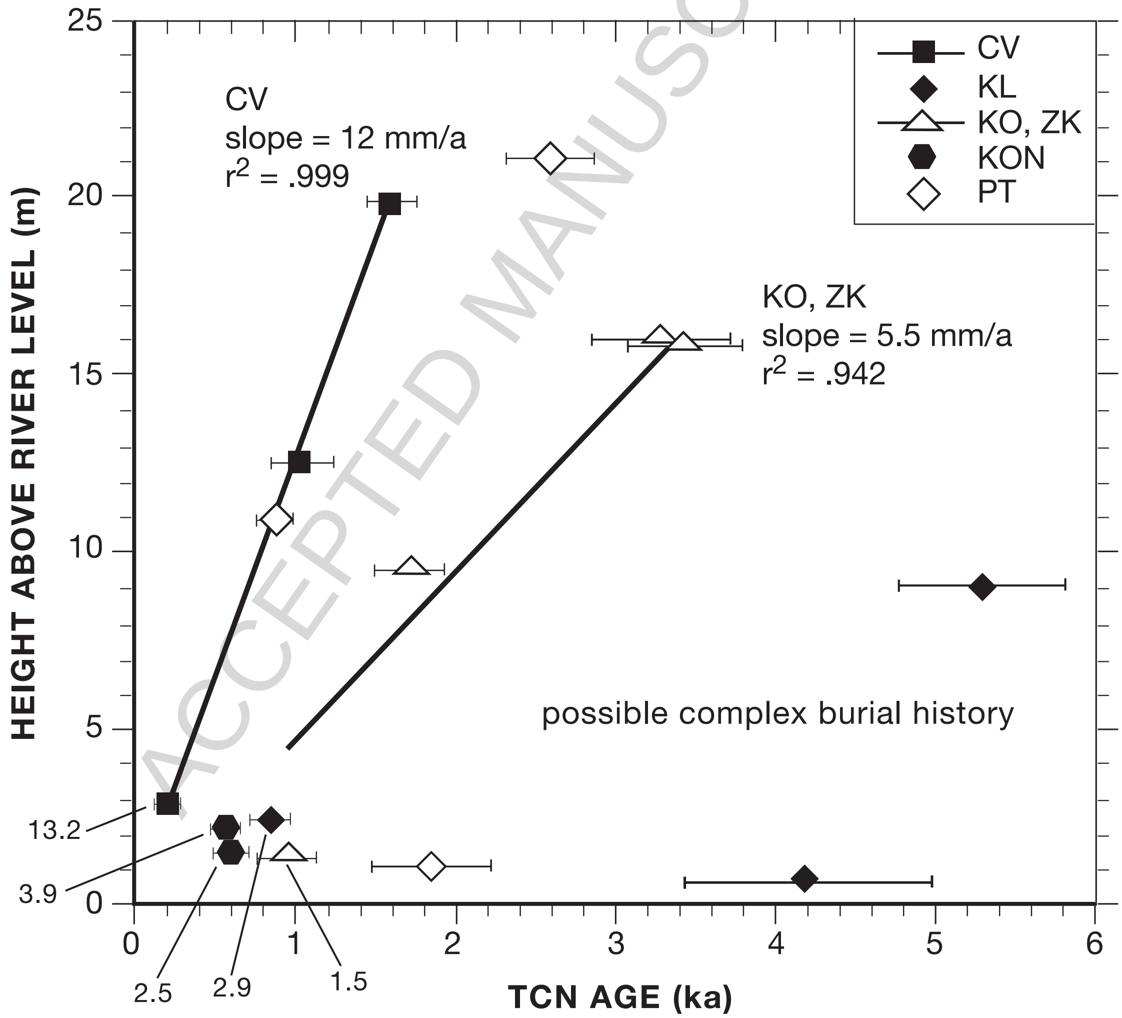

Table 1: AHe data.

Sample	Elev. (m)	Lat., N	Long., E	Lithology	# Grains	Mass (mg)	Ft	U ppm	Th ppm	MWAR	He pmol	Age (Ma)	Avg. (Ma)	% SD
HA1-1	3703	32.3037°	77.3795°	leucogranite	14	0.1060	0.82	15.0	4.0	69.8	0.0171	**2.35**	**2.51±0.29**	±11.6%
-2					3	0.0644	0.88	10.0	3.5	97.3	0.0094	**2.92**		
-3					13	0.0663	0.80	20.1	5.5	60.3	0.0249	_4.23_		
-4					6	0.1092	0.86	14.2	3.7	91.4	0.0168	**2.26**		
HA2-1	3882	32.2936°	77.3656°	leucogranite	15	0.0806	0.80	20.9	4.2	64.8	0.0133	**1.80**	**1.69±0.26**	±15.3%
-2					7	0.1793	0.87	9.7	1.9	105	0.0160	**1.93**		
-3					20	0.1025	0.79	11.7	1.7	59.5	0.0068	**1.33**		
-4					17	0.1203	0.82	11.7	2.5	67.3	0.0308	_4.91_		
HA4-1	4008	32.2719°	77.3311°	leucogranite	18	0.1298	0.81	12.6	2.2	63.3	0.0103	**1.44**	**1.39±0.04**	±2.7%
-2					19	0.1316	0.81	11.3	2.2	62.7	0.0089	**1.35**		
-3					18	0.0948	0.80	17.1	2.8	59.0	0.0097	**1.38**		
-4					18	0.0838	0.78	11.5	2.4	54.5	0.0705	_17.2_		
HA4b-2	4008	32.2719°	77.3311°	leucogranite	9	0.0144	0.68	6.9	1.5	34.3	0.0006	**1.65**	**1.52±0.14**	±8.9%
-3					10	0.0122	0.67	7.8	1.7	32.6	0.0005	**1.38**		
-4					11	0.0140	0.67	3.0	0.6	32.6	0.0003	_2.21*†_		
HA5b-1	3112	32.2859°	77.2614°	leucogranite	3	0.0557	0.87	11.4	2.6	88.6	0.0049	**1.61**	**2.14±0.53**	±24.9%
-2					9	0.0195	0.74	14.3	2.3	42.2	0.0032	**2.87**		
-3					8	0.0185	0.74	17.6	3.2	46.0	0.0025	**1.94**		
-4					10	0.0272	0.75	22.9	3.1	44.0	0.0703	_27.8_		
RH1-1	3300	32.3978°	77.2539°	leucogranite	10	0.0273	0.753	2.1	4.3	51.8	0.0008	**2.36†**	**1.98±0.39‡**	±19.5%
-2					10	0.0366	0.763	1.4	4.2	55.7	0.0031	_8.62†_		
-3					7	0.0467	0.829	2.3	14.3	80.3	0.0019	**1.59†**		
RH2-1	3171	32.3998°	77.2555°	leucogranite	4	0.0853	0.862	7.5	3.6	91.2	0.0034	**1.14**	**1.37±0.23‡**	±16.8%
-2					8	0.0492	0.786	10.0	1.8	57.6	0.0034	**1.60**		
-3					8	0.0298	0.768	9.8	1.9	54.0	0.0065	_5.33_		
-4					7	0.0411	0.807	10.9	2.0	64.8	0.0062	_3.16_		
RH3-1	3662	32.3893°	77.2528°	leucogranite	6	0.0481	0.817	1.5	3.5	68.2	0.0018	**3.72†**	**3.17±0.71‡**	±22.5%
-2					7	0.0575	0.828	1.4	4.9	71.4	0.0014	**2.29†**		
-3					7	0.0551	0.819	1.7	3.1	70.9	0.0015	**2.67†**		
-4					6	0.0458	0.826	2.4	11.3	67.5	0.0041	**4.01†**		
RH4-1	3911	32.3825°	77.2514	leucogranite	11	0.0154	0.676	0.8	1.5	38.6	0.0002	_2.94*†_	**1.68±0.16‡**	±9.3%
-2					9	0.0124	0.661	1.9	2.3	34.4	0.0004	_4.21*†_		
-3					8	0.0441	0.799	5.1	2.7	62.6	0.0019	**1.83**		
-4					11	0.0218	0.697	2.6	2.7	39.4	0.0039	**1.52†**		
CH1-1	3690	32.3314°	77.3962°	leucogranite	10	0.0052	0.615	7.4	2.7	28.2	0.0001	_0.78*_	**2.26±0.20‡**	±8.8%
-2					12	0.0108	0.680	6.1	4.1	33.4	0.0002	_0.85*_		
-3					15	0.0109	0.672	6.8	2.6	32.5	0.0007	**2.46**		
-4					9	0.0268	0.807	5.1	2.6	61.6	0.0013	**2.06**		

Elev. (m) – sample elevation
MWAR – mass weighted average radius of sample (μm)
% SD – standard deviation of average age as percentage of the average age
† – denotes poorly constrained age due to low U ppm (<3 ppm)
Ages in italics were considered outliers and not used for average age calculation.
Ft – alpha ejection correction after Farley et al. (1996)
Avg. – average AHe age (Ma)
‡ – denotes average age considered to have poor accuracy
* – denotes poorly constrained age due to low He pmol (<0.0004 pmol)

Table 2

Table 2. Sampling locations for strath terraces, topographic shielding factors, ^{10}Be concentrations, and ^{10}Be surface exposure dates.

Strath number	Sample ID	Latitude (±0.001N°)	Longitude (±0.001E°)	Altitude (m asl)	Height above river (m)	Shielding factor	^{10}Be (10^4 atoms/g of SiO_2)†	^{10}Be Exposure age (ka)*ǂ	^{10}Be Exposure age (ka)* #	Incision rate (mm/a)^
1	CV1	32.549	77.661	3568	12.54	0.92	4.65±0.73	1.04±0.19	1.12±0.20	12.1±2.4
1	CV2	32.549	77.661	3568	2.50	0.92	0.83±0.20	0.19±0.05	0.21±0.05	13.2±6.3
1	CV3	32.549	77.661	3568	19.85	0.92	7.21±0.33	1.61±0.16	1.71±0.17	12.3±1.4
2	KL1	32.542	77.368	3181	2.40	0.92	3.06±0.31	0.84±0.12	0.92±0.12	2.9±1.3
2	KL2	32.540	77.378	3189	9.04	0.92	19.23±0.61	5.29±0.51	5.36±0.51	1.7±0.3
2	KL3	32.537	77.381	3180	0.70	0.88	14.49±2.27	4.19±0.76	4.32±0.78	0.2±0.2
3	KO1	32.417	77.457	3108	1.39	0.93	3.35±0.60	0.95±0.19	1.03±0.20	1.5±1.1
3	KO2	32.418	77.448	3116	9.46	0.93	6.05±0.51	1.72±0.22	1.83±0.23	5.5±0.9
3	KO3	32.670	77.460	3122	15.85	0.93	12.24±0.55	3.44±0.35	3.61±0.36	4.6±0.6
3	ZK77	32.418	77.230	3135	16.00	0.91	11.01±1.45	3.28±0.43	3.46±0.54	4.9±0.7
4	KON2	32.640	77.348	3135	2.19	0.91	1.96±0.26	0.56±0.09	0.62±0.10	3.9±1.9
4	KON3	32.641	77.346	3129	1.49	0.91	2.06±0.32	0.59±0.11	0.65±0.12	2.5±1.8
5	PT1	32.467	77.548	3563	21.10	0.94	11.84±0.59	2.59±0.27	2.77±0.28	8.1±0.9
5	PT2	32.458	77.538	3599	10.85	0.89	3.92±0.32	0.88±0.11	0.96±0.12	12.3±1.9
5	PT3	32.471	77.545	3675	1.13	0.84	8.12±1.44	1.85±0.37	1.98±0.39	0.6±0.6

Note:
† Atoms of ^{10}Be per gram of quartz before application of shielding correction factor.
* Minimum ^{10}Be ages were calculated using sea-level high-latitude (SLHL) production rate = 4.98 ^{10}Be atoms/g quartz per year; zero erosion rate; and sample thickness of 2 cm; asl-above sea level. Shielding factor as calculated to correct for topographic barriers using the methods of Nishiizumi et al. (1989). TCN ages calculated using different scaling models produces ages of up to 20% older than those presented in this table and therefore these TCN ages should be considered as minimum estimates.
ǂ Minimum ^{10}Be ages were calculated using Lal (1991)/Stone (2000) time independent scaling factors.
\# Minimum ^{10}Be ages were calculated using Lal (1991)/Stone (2000) time dependent scaling factors.
^ Incision rate calculated using surface exposure ages determined using Lal (1991)/Stone (2000) time independent scaling factors and height above rivers incorporating 1 m error to account for survey errors and possible diurnal changes in river level.